



HAL
open science

On the attraction power of critical state in granular materials

Na Deng, Antoine Wautier, Yannick Thiery, Zhen-Yu Yin, Pierre-Yves Hicher,
François Nicot

► To cite this version:

Na Deng, Antoine Wautier, Yannick Thiery, Zhen-Yu Yin, Pierre-Yves Hicher, et al.. On the attraction power of critical state in granular materials. *Journal of the Mechanics and Physics of Solids*, In press, 149, pp.1-19. <10.1016/j.jmps.2021.104300>. <hal-03125580>

HAL Id: hal-03125580

<https://hal.inrae.fr/hal-03125580v1>

Submitted on 22 Jul 2021

HAL is a multi-disciplinary open access archive for the deposit and dissemination of scientific research documents, whether they are published or not. The documents may come from teaching and research institutions in France or abroad, or from public or private research centers.

L'archive ouverte pluridisciplinaire HAL, est destinée au dépôt et à la diffusion de documents scientifiques de niveau recherche, publiés ou non, émanant des établissements d'enseignement et de recherche français ou étrangers, des laboratoires publics ou privés.



Distributed under a Creative Commons CC BY-NC-ND 4.0 - Attribution - Non-commercial use - No Derivative Works - International License

1 On the attraction power of critical state in
2 granular materials

3 Na Deng¹, Antoine Wautier^{2*}, Yannick Thiery³, Zhen-Yu Yin⁴, Pierre-Yves Hicher⁵, and

4 François Nicot¹

5 ¹*Grenoble Alpes University, INRAE, UR ETGR, 2 rue de la Papeterie-BP 76, 38402*

6 *St-Martin-d'Hères, France*

7 ²*INRAE, Aix-Marseille University, UR RECOVER, 3275 Rte Cézanne, CS 40061,*

8 *13182 Aix-en-Provence Cedex 5, France*

9 ³*BRGM (French Geological Survey), Risk and Prevention Division, Orléans, France*

10 ⁴*Department of Civil and Environmental Engineering, The Hong Kong Polytechnic*

11 *University, Hong Kong, China*

12 ⁵*Research Institute in Civil Engineering and Mechanics (GeM), UMR CNRS 6183,*

13 *Ecole Centrale de Nantes, Nantes, France*

14 **Abstract**

15 The aim of this paper is to offer a fresh perspective on the classic con-
16 cept of critical state (CS) in granular materials by suggesting that CS can be

*Corresponding author

Email address: antoine.wautier@inrae.fr (Antoine WAUTIER)

17 defined through the use of a single proportional strain test. In classic con-
18 ventional testing, CS manifests itself under constant lateral stress and con-
19 trolled strain in one given direction whenever continuous shearing is applied
20 without change being induced to material volume. However, a comparison
21 between proportional strain tests and biaxial tests simulated with DEM
22 has clearly shown that the CS line (CSL) characterized by stresses, void
23 ratio and fabric indexes can act as an attractor. The mechanical responses
24 and fabric metrics evolve along dilatant proportional strain loading paths
25 according to similar values after the strain level has become large enough
26 to wipe out the material memory in the homogeneous domains considered
27 in this analysis, i.e., the shear band area in dense samples and the whole
28 area in loose samples. This suggests that the micro-structure of a granular
29 material subjected to any dilatant proportional strain loading paths evolves
30 while preserving its ability to withstand shearing without volume change at
31 any time. Therefore, the CS concept can be generalized to a wide class of
32 loading paths which shows that CS acts as a general attractor irrespective
33 of the loading path considered.

34
35 **Keywords:** Critical state; Shear band localization; Homogeneous domain; Propor-
36 tional strain loading path; Biaxial loading path; Granular materials; DEM simulation

37 1 Introduction

38 Although the structure of a granular material appears to be simple at the microscopic
39 scale, its behavior shows itself to be complex at the macroscopic scale, mostly due to

40 the collective rearrangement of particles. Based on the gain or loss of contacts, granular
41 materials will easily adjust to any change under loading conditions. Among the accessible
42 micro-structures, some have the ability to withstand constant shearing with no change of
43 volume. A state with such micro-structures is known as critical state (CS) and plays a
44 leading role in the most popular constitutive relations for granular materials. The concept
45 of critical state was first proposed by Casagrande [3] and developed by Roscoe et al. and
46 Schofield et al. [34, 37] in the form of a stationary state where stress and volume tend to
47 be constant under continuous shear strain. A steady stress ratio and a steady void ratio
48 are two conditions for this classical definition of critical state [41].

49

50 The CS concept is the basic principle behind critical state soil models [1, 2, 21] and
51 its importance in constitutive model cannot be underestimated, which explains its persis-
52 tence as a concept. Enormous efforts have been devoted to verifying the conjecture of the
53 uniqueness of the Critical State Line (CSL) [12, 47, 35] and to constructing appropriate
54 mathematical descriptions of CS to improve the capability of constitutive models [20, 23]
55 to simulate the mechanical behavior of granular materials. The evolution of internal soil
56 structures along physical tests have been analyzed for enriching constitutive models based
57 on micro mechanical investigations [19, 47, 14]. With the development of numerical tools,
58 such as the Discrete Element Method (DEM) [5], it has been possible to describe more
59 precisely micro-structures at critical state based on microscopic and mesoscopic descrip-
60 tions [11, 12, 17, 13, 18, 48, 16]. It has been observed that microscopic or mesoscopic
61 quantities such as metrics about fabric tensor and loop population also remain constant
62 at critical state [12, 48]. It can be shown that the difference between the actual porosity
63 and the CS porosity does not in itself determine the evolution of the micro-structure.
64 The coaxiality between the plastic strain rate direction and the fabric anisotropy proved

65 to be a relevant state variable in defining critical state [22, 41]. A third condition that
66 quantifies the role of fabric anisotropy in terms of its intensity and its relative orientation
67 with respect to loading direction should also be taken into account, in addition to the
68 aforementioned two conditions of constant stress ratio and void ratio [22, 41].

69

70 Research on CS is nearly exclusively based on conventional tests (triaxial tests in
71 3D or biaxial tests in 2D) in which a constant lateral stress condition $d\sigma_{\text{lateral}} = 0$ is
72 imposed together with a constant strain rate in one given direction $d\varepsilon_{\text{axial}} = \text{constant}$
73 [1, 2, 12, 13, 48]. This preferential selection is linked to the tendency of generating con-
74 stitutive models to work with stress and to calculate the resulting strains, as well as the
75 difficulty of imposing fully controlled strain paths in the laboratory [15, 8]. For con-
76 ventional loading, the $p - q$ path is preset; samples are loaded by increasing the axial
77 incremental strain under constant lateral confining pressure; volumetric strain and de-
78 viatoric stress responses are recorded according to the loading path. This test allows
79 for the existence of stationary states in volume and stress (the so-called critical state).
80 Proportional strain tests, on the other hand, have been much less studied whereby the
81 loading is imposed by proportional strain rates in the axial and lateral directions with
82 $d\varepsilon_{\text{lateral}} = \lambda d\varepsilon_{\text{axial}}$ and $d\varepsilon_{\text{axial}} = \text{constant}$. Under proportional strain loading condition,
83 the volumetric strain is no longer a response but a loading variable and the stress path is
84 not known beforehand, which makes the interpretation of such tests more complex than it
85 is for triaxial or biaxial tests. Except for the particular case of the undrained triaxial test,
86 whereby the volume is kept constant, the continuous change in volume prevents stationary
87 states in volume and stress along proportional strain paths to be observed. Without the
88 existence of a stationary state, investigating the evolution of the micro-structures along
89 a proportional strain loading path becomes a major challenge. In other words, tracking

90 the relation between triaxial (or biaxial) and proportional strain loading paths in terms
91 of mechanical responses and underlying micro-structures is an open and stimulating topic.

92

93 In order to generalize the concept of CS, we focus on the relation between the material
94 responses under dilatant proportional strain loading paths and biaxial loading paths in
95 2D. These two types of loading paths, as well as mixed biaxial/proportional strain paths,
96 have been simulated by DEM. The details of the DEM simulation are shown in Section 2.
97 Mechanical responses along biaxial tests and proportional strain paths are presented in
98 Section 3. The relation between proportional strain tests and biaxial tests in the $p - q - e$
99 space is analysed in Section 4. In Section 5, the fabric-related CS locus is studied. The
100 mechanical responses along the mixed loading paths are presented in Section 6, as is the
101 relation between the imposed dilatancy in proportional strain tests and the dilatancy in
102 biaxial tests.

103

104 **2 DEM simulation**

105 The Discrete Element Method (DEM) [5] is a powerful numerical method to simulate the
106 global behavior of a set of grains interacting through contact laws. It has been widely
107 used to simulate the mechanical response of granular assemblies under various loading
108 conditions. The mechanical states are characterized locally by kinematic information in-
109 cluding position, rotation and velocity of grains, as well as static information based on
110 contact force between contacting particles. In this study, the open source software YADE
111 [40] has been used.

112

113 Under consideration here is a quasi-2D soil sample in the form of an assembly of a
 114 single layer of 20,000 spherical particles contained within a surface domain of $1 \text{ m} \times 1.5 \text{ m}$.
 115 The particle sizes have an average diameter $d_{50} = 0.008 \text{ m}$ and $d_{\max}/d_{\min} = 2$. The elasto-
 116 frictional law introduced by [5] has been adopted as the contact law. The cohesiveless
 117 contact parameters between two grains contain a normal and tangential linear spring of
 118 respective stiffness k_n and k_t , as well as a friction characterized by a friction angle $\phi = 35^\circ$.
 119 k_n/D_s is given as 300 MPa, where $D_s = 2R_1R_2/(R_1 + R_2)$ and R_1, R_2 are the radii of
 120 particles in a given contact and k_t/k_n is 0.5. If the pressure of 100 kPa is considered, the
 121 average ratio of contact overlap and particle size $\langle u_n \rangle / d_{50}$ is around 0.16%, which is
 122 close to the value (10^{-3}) in literature [18, 41]. For sample preparation, two schemes can
 123 be used to obtain an isotropic compression of the specimen: the boundary moving scheme
 124 and the internal compacting scheme [45]. In this study, particles are enlarged, at first,
 125 while keeping the boundary walls fixed to generate a preliminary sample up to 90 kPa.
 126 Then, to achieve a more precise consolidation pressure, the sample undergoes an isotropic
 127 consolidation by imposing an equivalent incremental strain on the boundaries in the ver-
 128 tical and lateral directions up to a specific consolidation state. During this preparation
 129 process, contact friction angles of 2° and 35° are used to obtain dense and loose samples,
 130 respectively. Consolidation pressures of 10 kPa, 20 kPa, 40 kPa, 60 kPa and 100 kPa are
 131 considered. Three dense samples and five loose samples are thus prepared and named as
 132 indicated in Table 1. The void ratio is accounted for, based on solid and void surfaces
 133 on the 2D plane as shown in Fig.1. During the shearing process, a contact friction angle
 134 $\phi = 35^\circ$ is adopted in all the samples. Note that the soil mechanics convention is adopted
 135 throughout the paper with compression and contraction counted positive. As a result,
 136 dilatant/contracting volumetric strain are considered as negative/positive respectively.

137

138 For proportional strain tests, the **100kPa-dense** sample is used with an initial void
 139 ratio of 0.191. In the 2D simulation, $d\varepsilon_1 = \lambda d\varepsilon_2$ and $d\varepsilon_2 = 10^{-2} \text{ s}^{-1}$. As $d\varepsilon_v = (\lambda + 1)d\varepsilon_2$,
 140 $\lambda > -1$ corresponds to a contracting test, $\lambda = -1$ to a constant volume test, and $\lambda < -1$
 141 to a dilatant test. We have adopted $\lambda = -1.2, -1.3, -1.4$ for the three dilatant propor-
 142 tional strain tests. Biaxial loading paths with corresponding pressures are applied to all
 143 the samples indicated in Table 1. The stress and strain states are then described in 2D
 144 as follows: deviatoric stress $q = \sigma_2 - \sigma_1$, mean stress $p = (\sigma_1 + \sigma_2)/2$, and volumetric
 145 strain $\varepsilon_v = \varepsilon_1 + \varepsilon_2$, where σ_1 and σ_2 are the principal stresses at horizontal and vertical
 146 directions and ε_1 and ε_2 are the principal strains. The direction 2 is always the vertical
 147 loading control direction ($\dot{\varepsilon}_2 = 10^{-2} \text{ s}^{-1}$), as shown in Fig.1. When the pressure ranges
 148 from 20 kPa to 200 kPa, the Inertial Number I of the granular system ranges among
 149 $2.77\text{e}10^{-5} - 8.76\text{e}10^{-5}$, which corresponds to a quasi-static state [6].

150

151 In reality a 2D model of a granular material is quantitatively different from sand
 152 assemblies; for example void ratio values and coordination numbers in 2D assemblies are
 153 smaller than those in 3D [12], and stresses expressed in kPa relies on the use of an arbitrary
 154 out of plane dimensionⁱ. However, given that the complexity of the constitutive behaviour
 155 of granular assemblies stems mainly from the local properties and the disordered packing,
 156 both effects can be captured in 2D simulations [30]. Qualitative investigations of granular
 157 materials based on DEM simulations in 2D can then be considered as both effective
 158 and efficient. Proof of such effectiveness and efficiency can be found in various studies
 159 of the microscopic mechanism behind the mechanical responses of granular materials
 160 under different loading paths have been investigated [12, 17, 13, 48, 25]. Thus, the 2D

ⁱIn the present study, the out of plane dimension is then taken equal to the thickness of the sample box (0.04 m), which allows kPa rather than kN/m to be used for the stress unit on the boundary walls. The thickness of the box has a proportional influence on the stress values, which should not impact the following results, at least qualitatively.

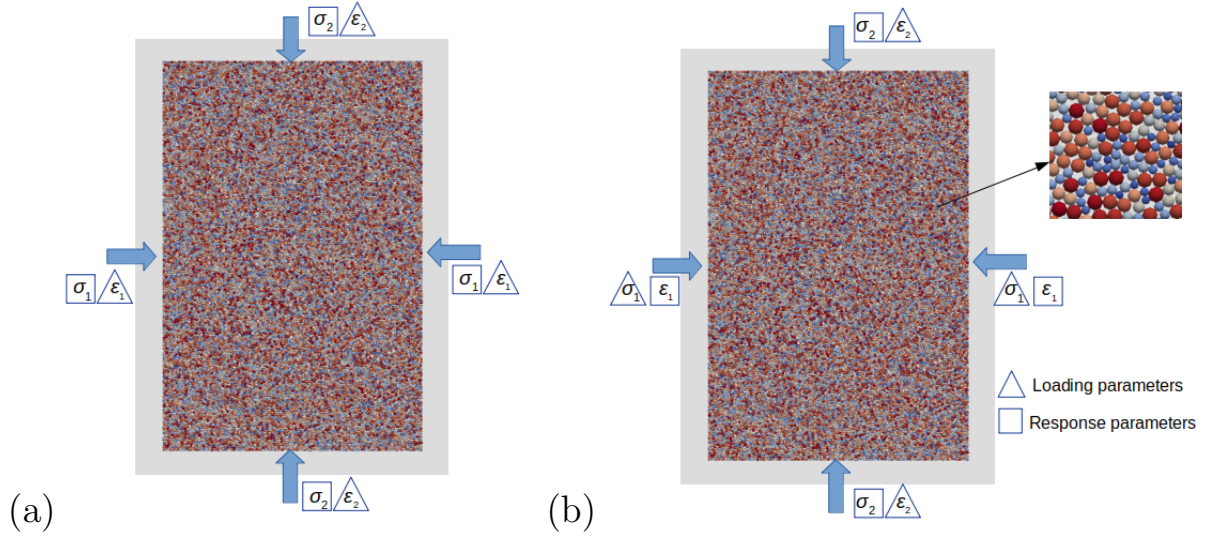


Figure 1: Quasi-2D DEM specimens for (a) proportional strain tests where loading parameters are ε_1 and ε_2 and (b) biaxial tests where loading parameters are ε_2 and σ_2 . The direction 2 is always the vertical loading control direction at the REV scale.

161 assembly simulation is adequate enough for qualitative investigations of critical states under proportional strain and biaxial loadings performed in this study.

Table 1: Initial void ratios e_0 of prepared samples. The sample '100kPa-dense' is used in proportional strain tests)

Sample	40kPa-dense	60kPa-dense	100kPa-dense	10kPa-loose
e_0	0.197	0.195	0.191	0.266
Sample	40kPa-loose	60kPa-loose	100kPa-loose	20kPa-loose
e_0	0.267	0.265	0.261	0.267

162

3 Mechanical response

3.1 Mechanical response along dilatant proportional strain loading paths

3.1.1 Stress-strain analysis

Figure 2 shows the evolution of the deviatoric stress q along the axial strain ε_2 under dilatant proportional strain loading path with $\lambda = -1.2, -1.3, -1.4$. In this figure, it can be observed that the deviatoric stress q grows quickly at first and then decreases after the peak. Gradually, q decreases to 0. When $\lambda = -1.4$, the sample undergoes the fastest dilatancy and the corresponding stress curve reaches the earliest peak at $\varepsilon_2 = 0.013$ and the earliest zero deviatoric stress at $\varepsilon_2 = 0.061$. When $\lambda = -1.3$ and $\lambda = -1.2$, it appears that the peaks are reached at $\varepsilon_2 = 0.017$ and $\varepsilon_2 = 0.019$ because of smoother and smoother dilatancy. Zero mean pressure p occurs at $\varepsilon_2 = 0.085$ and $\varepsilon_2 = 0.142$, respectively.

3.1.2 Kinematic pattern: from localization to diffuse

The existence of a stress peak (Fig.2) corresponds to a generalized limit state [29] which has been shown to be a proper failure state [43]. Various failure modes, characterized by localized or diffuse patterns, can be encountered after the peak, along the descending branch. In biaxial tests, either diffuse or localized modes will appear [29]. In this study, however, these two modes appear successively along each proportional strain test. In this subsection, the incremental deviatoric strain distribution has been used to characterize the kinematic pattern, as introduced in literature [33, 48]. For example, in the test with $\lambda = -1.2$, a typical diagonal shear band traversing the whole specimen appears at $\varepsilon_2 = 0.008$, as shown in Fig.3 (I), corresponding to the point I in Fig.2. After a process

185 of dilatancy, the shear band begins to vanish in the strain state $\varepsilon_2 = 0.110$ shown in
186 Fig.3 (II). Fig.3 (III) demonstrates the kinematic pattern when $\varepsilon_2 = 0.142$, where the
187 mean pressure p is close to zero. An evolution from localization, when the strain largely
188 concentrates in a partial domain of the material, to liquefaction, when the effective stress
189 within the granular specimen is reduced to essentially zero, has been observed along the
190 three dilatant proportional strain paths, as shown in Fig.3. With the increase in volume
191 along the loading path ($\lambda < -1$), the density of the sample gradually decreases and the
192 kinematic pattern changes from localized to diffuse until a zero mean pressure p is reached.

193

194 Kinematic patterns characterize the nature of the failure mode, together with the
195 spatial domain. It has been widely accepted that fabric-related measures should be taken
196 either within the shear bands or within the full sample when the shear deformation is
197 diffuse, since measures within nonhomogeneous domains have no constitutive meaning
198 [10, 12, 13, 48, 35]. In this study, the index M_{ed} [24] has been adopted to define the shear
199 band domain. M_{ed} refers to an absolute difference of incremental deviatoric strain inside
200 and outside the shear band with a trial width divided by their sum. Regarded as an op-
201 timization problem, the shear band width has been obtained according to the maximum
202 M_{ed} within a reasonable range of the trial shear band width. More details are available
203 in [24]. In the following section, labels with * refer to measures within a homogeneous
204 domain (shear band for dense specimen and whole sample for loose specimen). Taking
205 the kinematic evolution as its base, the next section will examine the evolution of the
206 stress and void ratio.

207

3.2 Mechanical response along biaxial loading paths

As recalled in the introduction, the critical state (CS) refers to a state where stresses, void ratios and fabrics tend to be steady at relatively large deformation when shear strain further increases [41]. Biaxial tests used as references have been simulated to define the critical state line which refers to a collection of critical states obtained at different confining pressures. Typical macroscopic responses in biaxial tests are illustrated in Fig.4, where deviatoric stress and volumetric strain evolve with respect to axial strain ε_2 . Figures on the left hand show the results from the dense samples. In these three figures, the deviatoric stresses show an increase before a peak is reached, and a decrease followed by a steady regime with small fluctuations. The stress peaks rise gradually with the increase in confining pressure from 40 kPa to 100 kPa. The volumetric strain shows a small contractancy, at first, and transfers to dilatancy before a steady state is reached. On the other hand, for the loose specimens, q and ε_v continuously rise up to steady states, as shown on the right-hand panel of Fig.4. Localized and diffuse patterns have developed within the dense and loose samples, respectively.

As highlighted in Subsection 3.1.2, it is important to focus on the domain within the shear band when considering void ratio and fabric indexes in order to characterize material scale properties by considering only homogeneous domains. The same point holds for stresses even if the stress heterogeneity is never reported in strain localization problems. Do stress patterns exhibit significant differences inside and outside the shear band? Is the stress path within the shear band the same as in the whole sample? Usually, stresses are obtained macroscopically from the external forces applied on the sample boundaries. To obtain the stresses within shear band, we have adopted a local definition based on Love-Weber stress at the grain scale. The mean stress tensor $\bar{\sigma}_{ij}^p$ of each particle can be

233 computed based on the contact forces applied, thanks to the Gauss theorem [31, 26]. More
 234 details are available in aforementioned literature. The stress tensor for a given domain Ω
 235 can be computed based on all N_p particles in the domain as $\sigma_{ij}^* = \frac{1}{\Omega} \sum_{p=1}^{N_p} \bar{\sigma}_{ij}^p V^p$.

236

237 In Figure 5, global stress components have been compared with local stresses com-
 238 puted within the shear band domain for the 100kPa-dense sample under a biaxial loading
 239 path. Stresses based on boundaries, including principal stresses σ_1 and σ_2 in the whole
 240 sample, are compared with σ_1^* and σ_2^* considering the domain of the shear band based
 241 on the grain scale stress definition. In addition, the relative orientation of the stress ten-
 242 sor characterized by $(\theta_{\sigma_1^*} - \theta_{\sigma_1})$ is presented. It is observed that the evolution of stresses
 243 within the shear band and the whole sample is far more similar than it is for the void ratio
 244 [48] in 2D. Thus, it is reasonable to adopt stresses based on sample boundaries instead of
 245 stresses within the shear band when investigating critical state. This approach has been
 246 adopted throughout the rest of this paper. A precise characterization of the loading path
 247 within the shear band and its difference from the whole specimen is an issue that remains
 248 to be examined. At the moment, it is beyond the scope of this paper. Some preliminary
 249 results on stress rotation within shear bands can be found in Liu et al. [25] and more
 250 investigations and discussions on this issue will be conducted in further studies.

251

252 4 $p - q - e$ space analysis

253 The CSL is characterized by mean stress p , deviatoric stress q and void ratio e , usually
 254 plotted separately in planes (p, q) and (p, e) . So, here, mechanical responses (p, q, e) from
 255 proportional strain tests and biaxial tests have been compared in $p - q$ and $p - e$ planes.

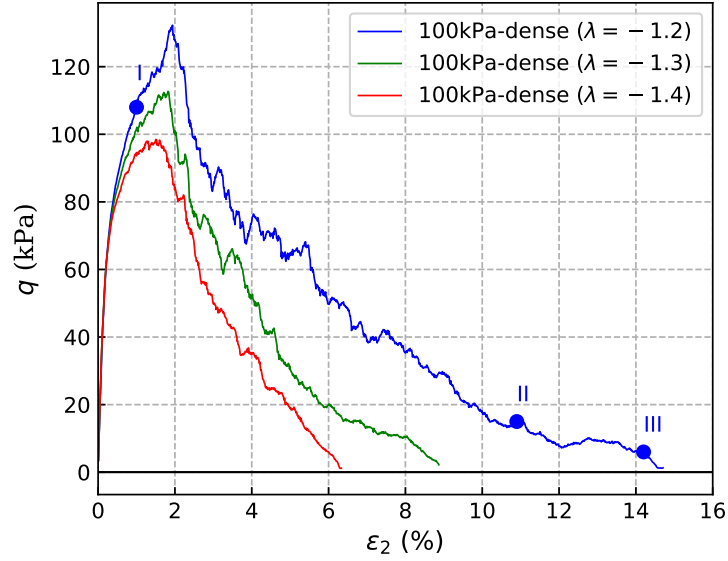


Figure 2: Evolution of the deviatoric stress q along dilatant proportional strain tests with different magnitudes of dilatancy characterized by $\lambda = -1.2, -1.3, -1.4$. Point I, point II and point III refer to onset of a well marked shear band at $\varepsilon_2 = 0.010$, slightly blurred shear band at $\varepsilon_2 = 0.109$, and the pressure p close to zero at $\varepsilon_2 = 0.142$, respectively. The corresponding kinematic patterns of these three points are shown in Fig.3

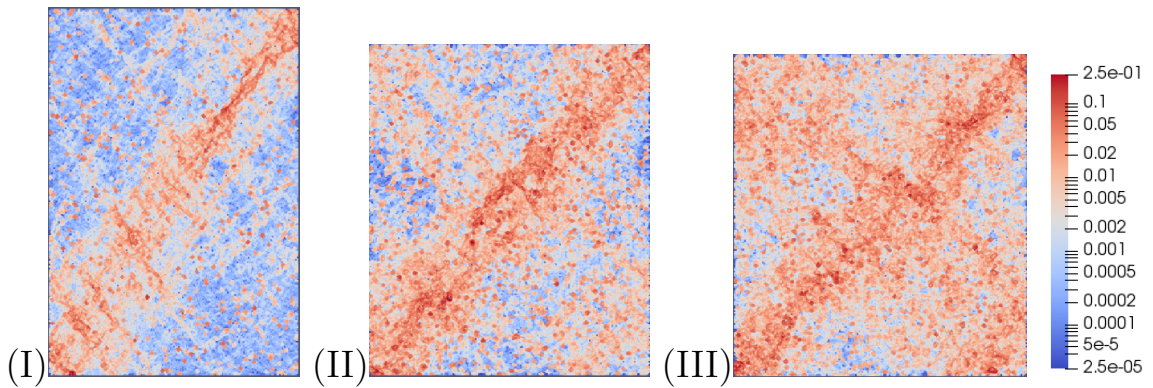


Figure 3: Incremental deviatoric strain maps ($d\varepsilon_d$) estimated for axial strain increments of 0.11%. Three axial strains are considered along the proportional strain path $\lambda = -1.2$: (I) onset of a well marked shear band at $\varepsilon_2 = 0.010$, (II) slightly blurred shear band at $\varepsilon_2 = 0.109$, (III) just before liquefaction (p is close to 0) at $\varepsilon_2 = 0.142$. The corresponding points in $q - \varepsilon_2$ plane are shown in Fig.2

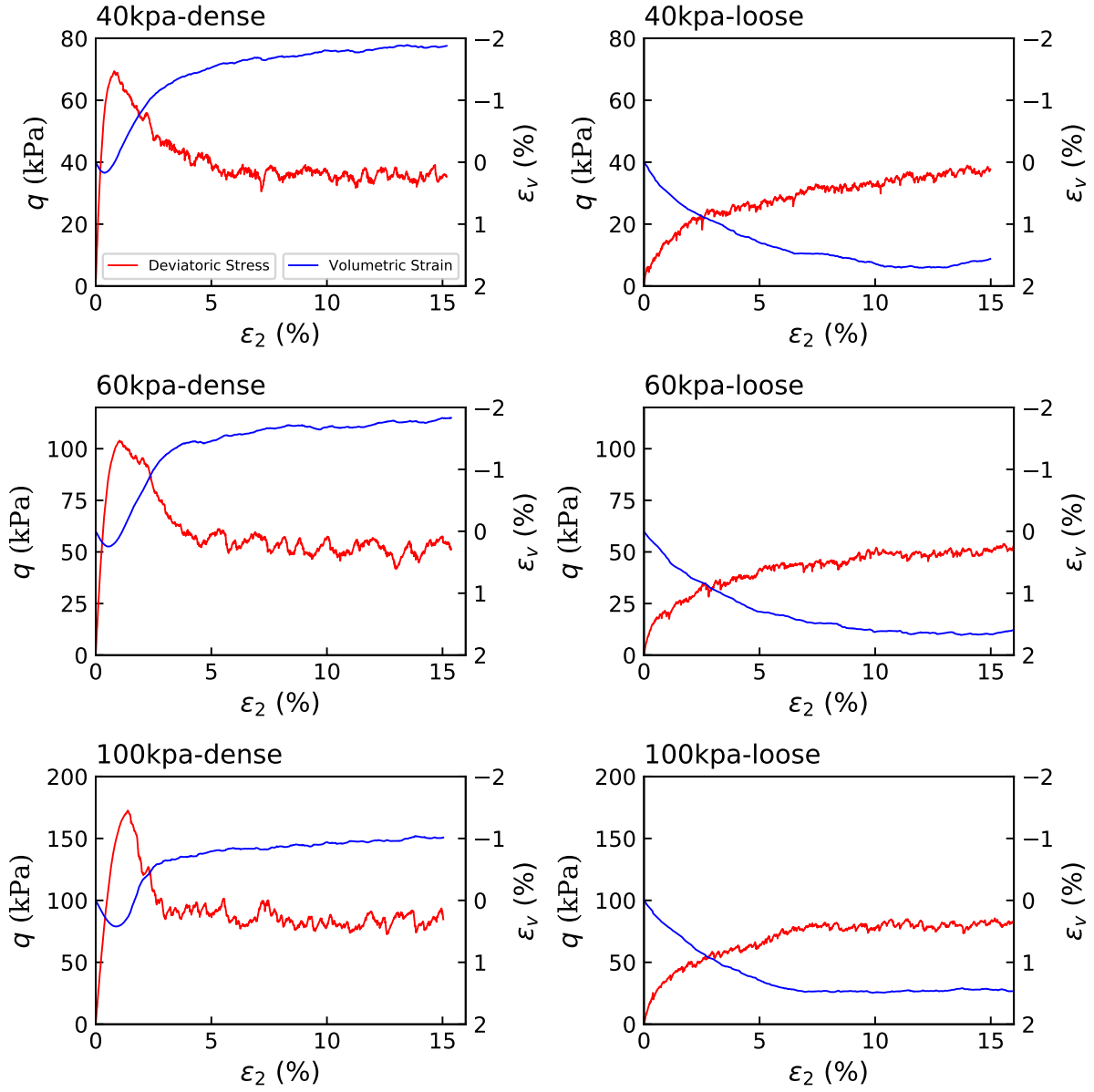


Figure 4: Deviatoric stress and volumetric strain of biaxial tests in dense (left panel) and loose (right panel) samples. Three biaxial loading paths with $\sigma_0 = 40$ kPa, 60 kPa and 100 kPa are considered. Note that soil mechanics convention is adopted with positive compression.

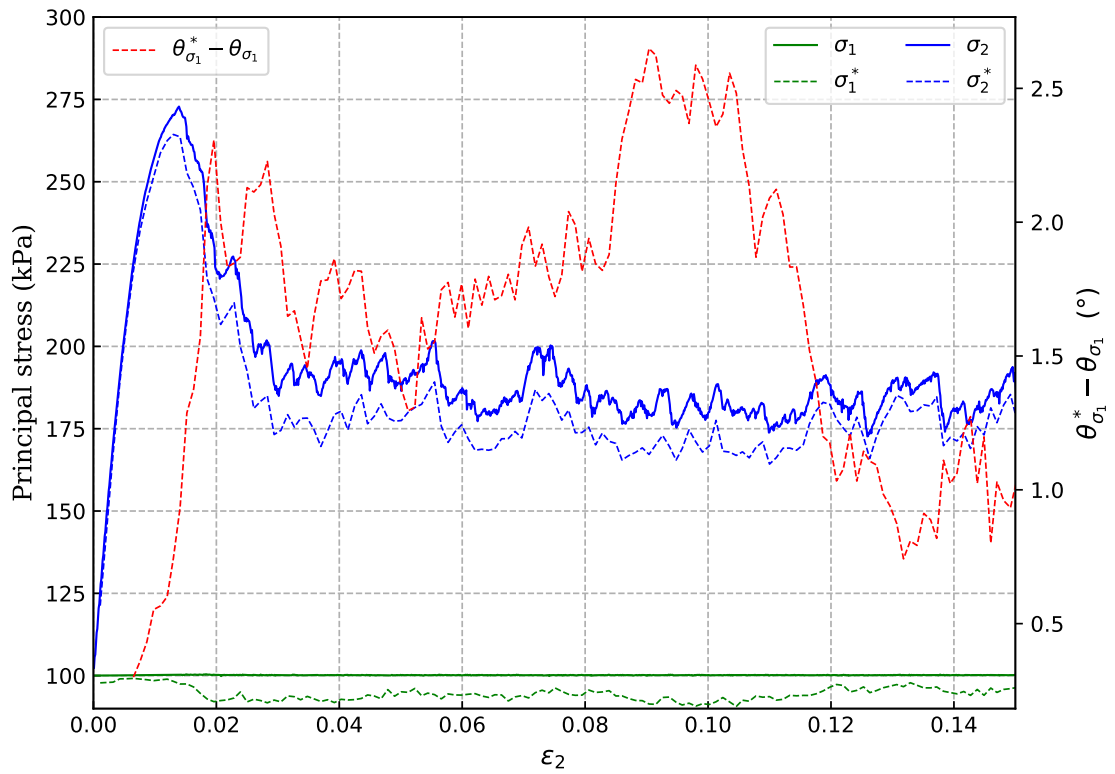


Figure 5: Principal stresses in the whole sample (σ_1 and σ_2) and within the shear band (σ_1^* and σ_2^*), and relative orientation of principal stress ($\theta_{\sigma_1}^* - \theta_{\sigma_1}$). The 100kPa-dense sample under biaxial loading path is adopted.

256 4.1 $p - q$ plane

257 Figure 6 illustrates the stress paths of the biaxial tests and the proportional strain tests.
258 The three straight lines result from biaxial tests with dense samples. The initial states
259 are marked with triangles and ultimate points are highlighted by squares labelled as A, B
260 and C. The critical stress ratio line (CSRL) is given as a dashed line based on the three
261 ultimate points, and the three highest points define the maximum stress ratio line (MSRL).

262

263 As for the dilatant proportional strain tests, Fig.6 shows that the path of the devia-
264 toric stress and the mean stress (p, q) for each case, starts from the initial state of around
265 (100 kPa, 0), evolves to the MSRL and, at the end, changes direction to turn back toward
266 the zero-stress level along an asymptotic line after having formed a 'loop'. Result of a
267 mixed biaxial test/proportional strain test is also presented in Fig.6. The sample was led
268 to CS by a biaxial loading under 100kPa lateral stress upon which the loading mode was
269 switched to a dilatant proportional strain loading. It can be seen that the stress path
270 evolves from the very beginning along the CSRL with decreasing p and q .

271

272 Figure 5 illustrates that the stresses in the sample are relatively homogeneous at least
273 in a 2D condition. The vanishing of the principal stresses along the dilatant proportional
274 tests occurs simultaneously with the evolution from localized to diffuse failure (Figure 3).
275 The vanishing of the principal stresses offers two possibilities: (1) liquefaction occurs only
276 within the shear band and the behavior outside the shear band is regarded to be close to
277 an elastic solid under unloading; (2) the kinematic pattern evolves gradually to become
278 diffuse throughout the whole sample. In addition, it is worth noting that all computed
279 results display an asymptotic behavior in the $p - q$ plane, approaching the CSRL inde-
280 pendently of the imposed dilatancy ratio, as shown in Fig.6. This kind of stress track,

281 especially the loop, has scarcely been reported in the literature for dilatant proportional
282 strain tests in either laboratory [15, 39, 7] or DEM simulations [32], with exception of the
283 work reported by [4, 44, 8].

284

285 To further refine the classification of the stress response along proportional strain
286 paths, a variety of proportional strain paths have been additionally simulated using spec-
287 imens with different densities. The results are shown in Fig.7. Based on these results,
288 the stress response path along proportional strain tests can be categorized into four types
289 under different densities and volumetric strain rates, as illustrated in Fig.8. Group 1 re-
290 sults from one typical contracting strain path along which p and q increase continuously,
291 and Group 2 comes from a typical dilatant proportional strain path leading to zero mean
292 pressure p [7, 27]. Group 3 represents stress paths from a dense sample under proportional
293 strain tests with a relatively small dilatant rate, whereas Group 4 demonstrates a stress
294 path under a proportional strain test with a contracting rate in a dense sample, similar
295 in trend to the stress path under an undrained loading.

296

297 It is worth paying attention to Group 3 because of the infrequently-reported 'stress
298 loop'. A dense sample with imposed dilatancy was experimentally investigated by Ibrahim
299 et al. [15], Chu et al. [4] and Daouadji et al. [8], and numerically by Wan and Guo [44]
300 and Nicot et al. [32]. The $p - q$ relation from [15] along such a loading path has been
301 drawn in Fig.8. The stress path was stopped early with an axial strain of around 5%. If
302 the test had been conducted further, with the growth of volume and a constant number of
303 particles, an increasing number of contacts would probably have opened that would have
304 resulted in a stress drop at some point. Indeed, the complete increase and decrease in q
305 along such a loading path reported in [8] produced a stress path that was more like a back-

306 and-forth line than a loop. This may have been the case because it was a middle dense
 307 sample with a not very pronounced softening. Both the limited shearing strain and the
 308 use of the middle dense samples could explain why no such loops were observed, even for
 309 similar loading conditions [32]. Such loops were, however, reported in [44, 38]. The Group
 310 3 type has also been obtained in 3D simulations not included in this paper which focuses
 311 on 2D simulations. It would be worth to conduct a detailed 3D investigation in the future.

312

313 As for the type of Group 4, stress softening was observed both along isochoric and
 314 contracting proportional strain loading paths. The slight decrease in the deviatoric stress q
 315 is linked to strain localization within the sample, since shear bands were generated in these
 316 two simulations. As underlined in [44], the slope of the stress path under a contractant
 317 proportional strain loading depends on the volumetric strain rate. But, according to the
 318 results in Fig.6, the critical stress ratio in proportional strain tests is independent of λ
 319 when the axial strain is large enough, as shown in Fig.6.

320 4.2 $p - e$ plane

321 Void ratios e^* within the shear band are tracked for dense samples, and global void ratios
 322 e^* for loose samples. The void ratio is given in 2D by $e^* = (A_{sb} - A_s)/A_s$, where A_{sb} and
 323 A_s denote, respectively, the total and solid areas of the shear band. The evolution of e^*
 324 is represented in Fig.9, with respect to mean stress p .

325

326 As for proportional strain tests shown in Fig.9 (a), the results converge to a master
 327 curve in the $p - e^*$ plane independent of the dilatant rate characterized by λ . When the
 328 starting point of the proportional strain loading is at critical state under a biaxial loading,
 329 the (p, e^*) curve will follow the master curve from the very beginning of the proportional

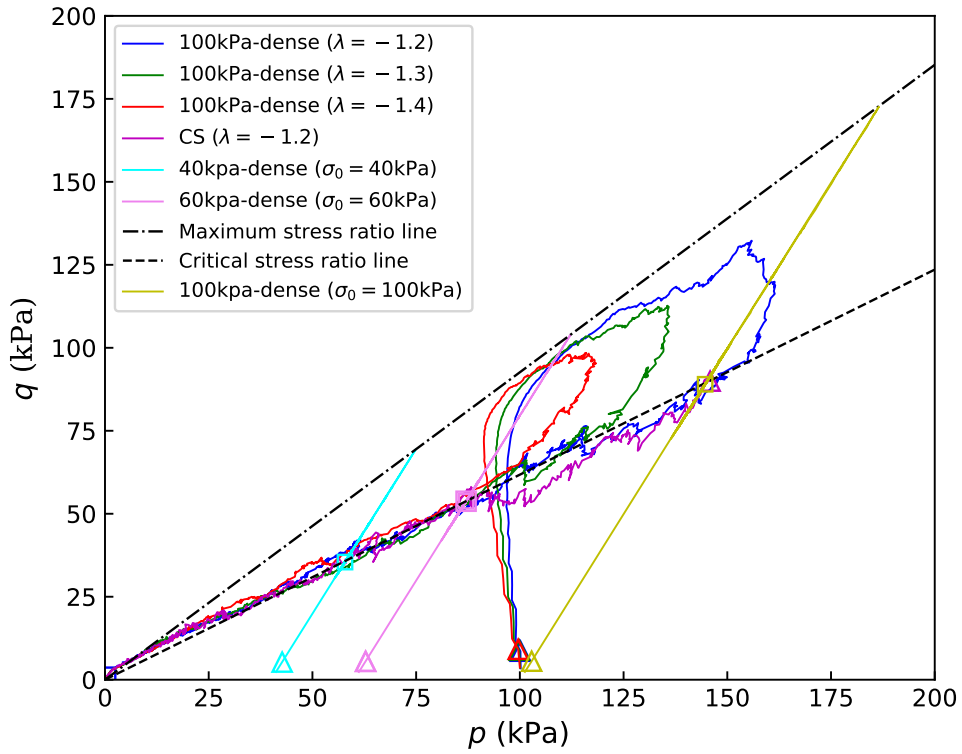


Figure 6: Stress paths of biaxial tests and proportional strain tests in $p - q$ plane. The start and end points are marked by triangles and squares, respectively. The critical stress ratio curve and the maximum stress ratio curve are drawn according to the critical states and the maximum value from biaxial tests, respectively.

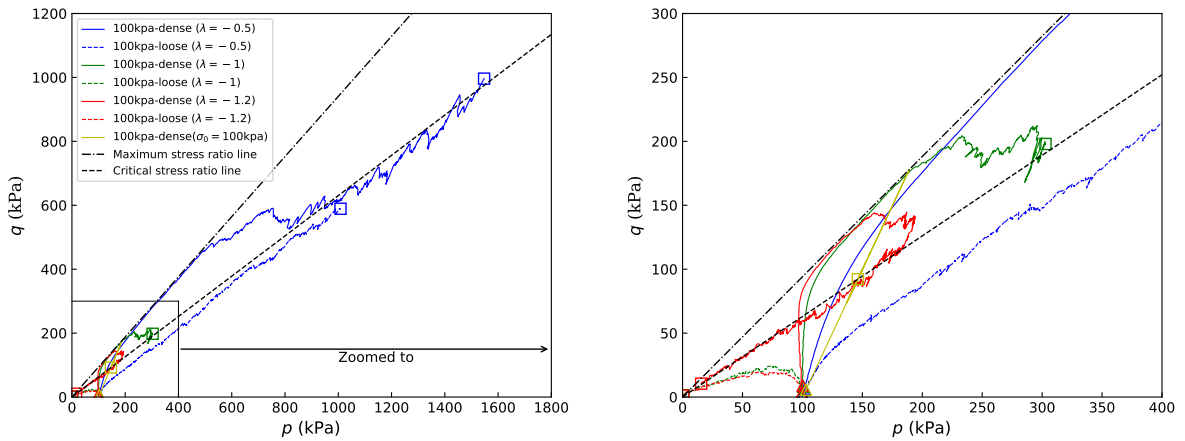


Figure 7: Stress paths in $p - q$ plane along six proportional strain tests and one biaxial test. Dilatant ($\lambda = -1.2$), undrained ($\lambda = -1$) and contracting ($\lambda = -0.5$) proportional strain paths are conducted with the samples labelled 100kPa-dense and 100kPa-loose. A biaxial loading path is performed in the sample 100kPa-dense. The square domain is zoomed up on the right hand side.

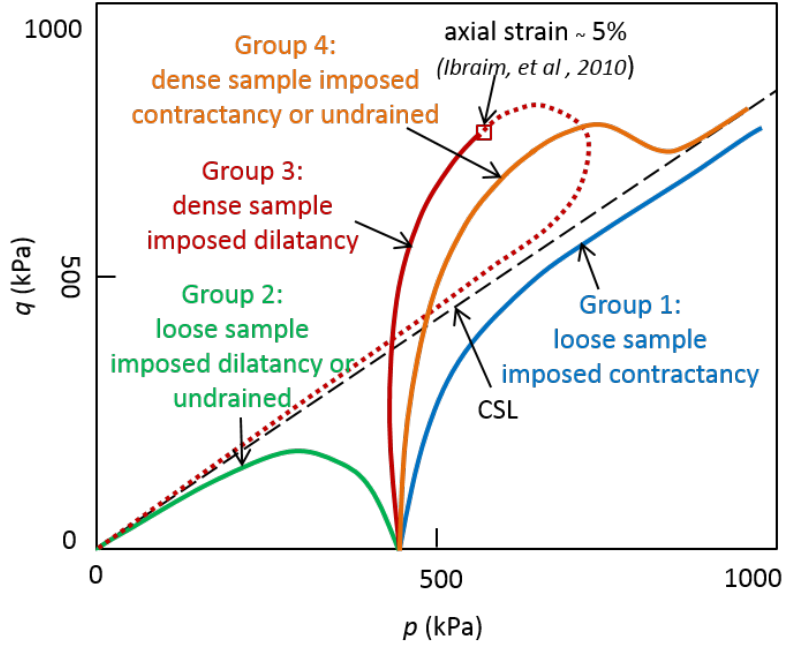


Figure 8: Four categories of stress path along proportional strain tests according to DEM simulation results shown in Fig.7.

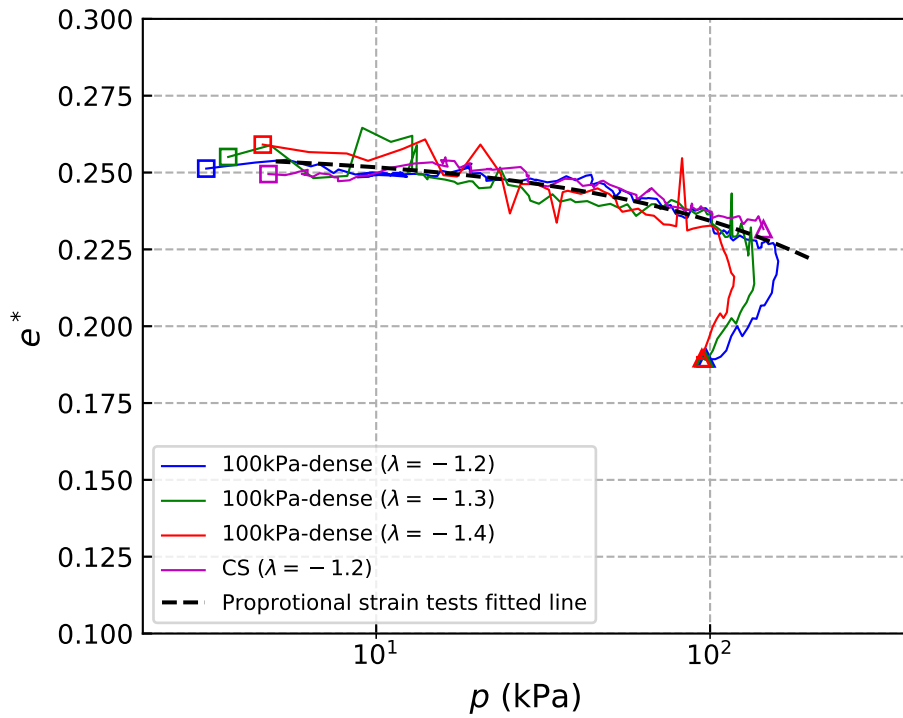
330 strain loading.

331

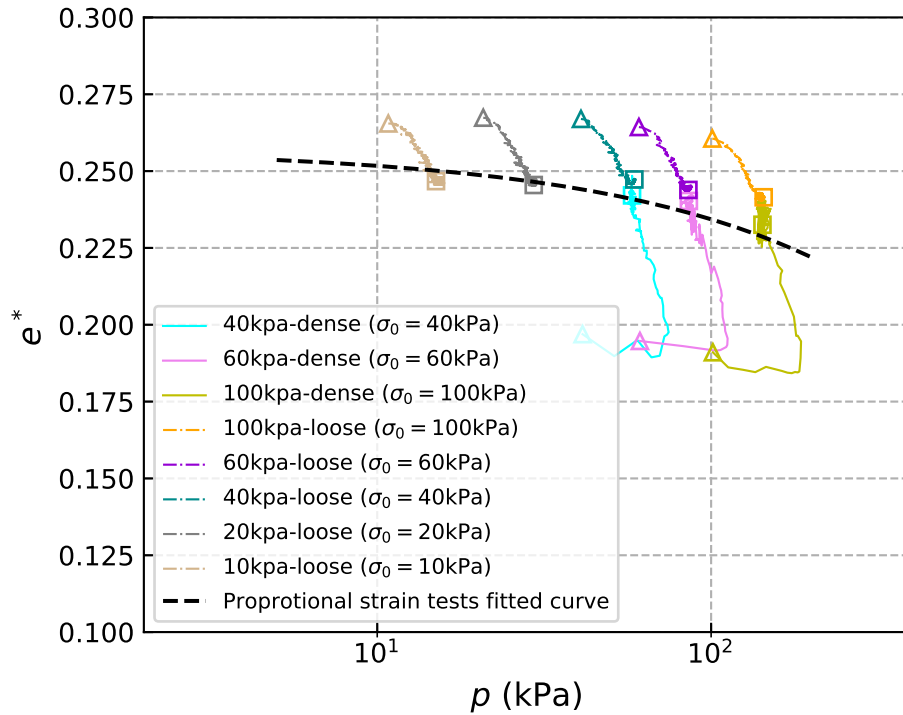
332 As for biaxial tests with confining pressures of 40 kPa, 60 kPa and 100 kPa, the results
 333 illustrated in Fig.9 (b) are consistent with experimental observations in [10] and DEM
 334 simulations in [48]. Namely, e^* from dense samples, after dilatancy, evolves to meet e^* of
 335 loose samples at the critical state. For a more precise representation of the CSL in the
 336 (p, e^*) plane, two biaxial test results with confining pressures at 10 kPa and 20 kPa have
 337 been included.

338

339 These critical states with proportional strain tests in $p - e^*$ plane are compared. An
 340 interesting feature stands out: the fitting curve of $p - e^*$ from proportional strain tests
 341 crawls just along the critical state curve obtained from the biaxial tests. Even though the
 342 CS from nine biaxial tests can lead to the critical state line, the master curve obtained
 343 from fitting a curve to a cluster of $p - e^*$ data in dilatant proportional strain tests, com-



(a)



(b)

Figure 9: $p - e^*$ evolution in proportional strain (a) and biaxial (b) tests. The start and end points are marked by triangles and squares, respectively. A fit based on a power function is shown for proportional strain tests and repeated to compare with the results from biaxial tests, as all dilatant proportional strain tests converge towards a master curve. The equation of the fitted curve is $e^* = 0.2571 - 0.02275\left(\frac{p}{100}\right)^{0.6274}$.

344 pared to the nine CS obtained from biaxial tests, induces less uncertainty.

345

346 It is worth noting that the fitting curve is based on a power function rather than
347 a logarithmic function. It has been proved experimentally [42, 23] that, unlike in clay,
348 the critical state line for granular materials cannot be estimated by a straight line in the
349 $e - \log p$ plane. Thus, the commonly used CSL expression $e_c = A + B \ln p_c$ is generally
350 not representative for granular materials, where the e_c and p_c are the critical void ratio
351 and the critical pressure; A and B are two constants characterizing a given material. The
352 relation of e_c and p_c for granular materials can be expressed as $e_c = D - E \left(\frac{p_c}{F}\right)^G$, where F
353 is a reference pressure, usually the atmospheric pressure (101 kPa) for convenience, and
354 D, E, and G are dimensionless constants that can be identified from experiments on a
355 given material [20, 46].

356

357 In summary, from Fig.6 and Fig.9, it can be observed that the master curves (p, q)
358 and (p, e^*) from dilatant proportional strain tests agree well with the critical state lines
359 from biaxial tests after a sufficiently large strain level has been imposed (or immediately
360 if the initial state is already a critical state). Hence it is shown that the classical critical
361 state surface defined in $p - q - e$ space for a given granular materials can be obtained by
362 performing one single dilatant proportional strain test. To the best of our knowledge, no
363 such results have been reported in the literature. For a further analysis of this relation,
364 the following sections will investigate the micro/meso-structures of the samples under pro-
365 portional strain and biaxial tests, as well as under mixed biaxial/proportional strain tests.

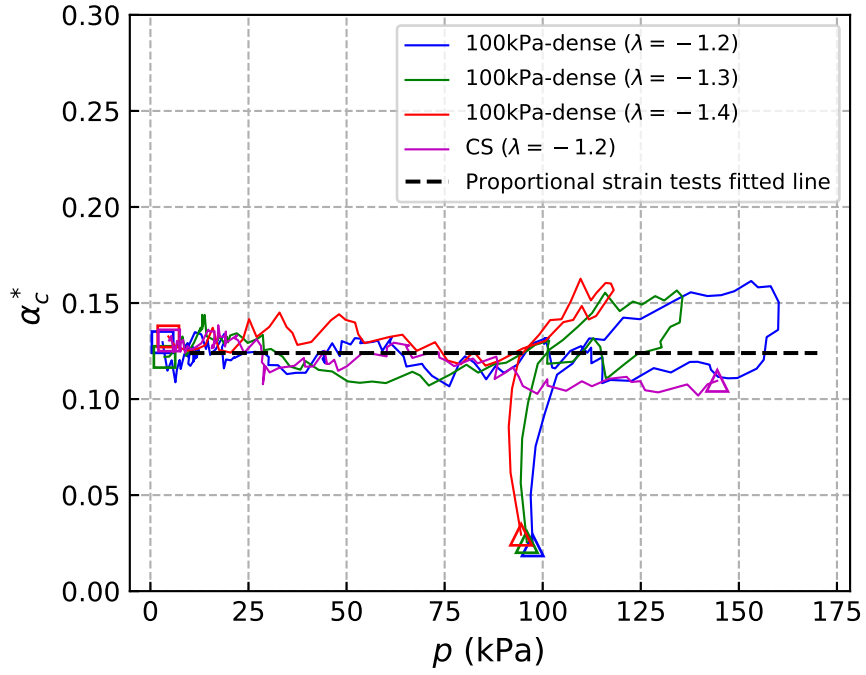
366

5 Fabric-related critical state locus

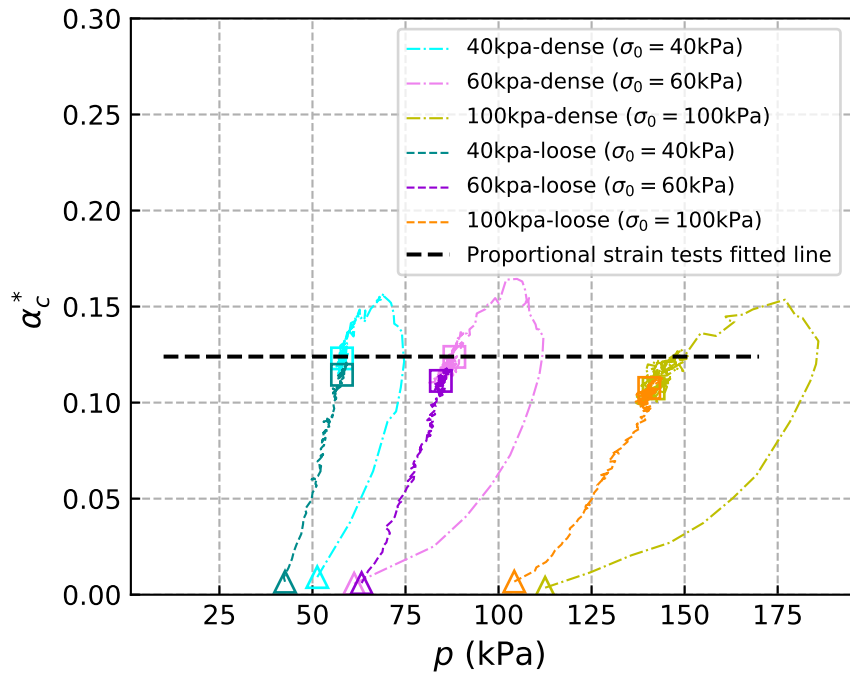
Even though the critical state is most often characterized by the relation between the mean stress p , the deviatoric stress q and the void ratio e when stress and strain rate directions are fixed [41], the evolution of the fabric is also an important feature to be added to the $p - q - e$ space in order to stay within the framework of Anisotropic Critical State Theory (ACST) that requires the values of the fabric to be steady.

5.1 Fabric tensor analysis

A fabric tensor quantifies micro-structural orientation-related characteristics of the material in a tensorial form [13]. In this subsection, the inter-particle contact normal directions are characterized by the second-order fabric tensor of $F_c = \frac{1}{N_c} \sum_{k=1}^{N_c} n^k \otimes n^k$, where N_c is the total number of inter-particle contacts in the assembly; n^k is the unit vector representing the normal direction of the k th contact. Only contacts in the shear band are considered. The norm of the normal at contact has to be normalized by the Lode angle in order to be unique in 3D. In the present 2D case there is no Lode angle; thus, no need for normalization. To make sure that the CS investigated within shear bands satisfies the third condition required by ACST as mentioned in Section 1, the orientation of the fabric tensor has been compared with the direction of the plastic flow which can be related to the stress tensor for monotonic radial loading [22]. The deviatoric orientation is less than 2.5 degrees throughout the whole biaxial test on the 100kPa-dense sample. The variable α_c^* , referring to the difference between the two principal components of F_c^* within the shear bands, is measured to characterize fabric anisotropy. $\alpha_c^* = 0$ refers to an isotropic fabric, whereas $\alpha_c^* = 1$ corresponds to the situation that the normal direction of all inter-particle



(a)



(b)

Figure 10: $p - \alpha_c^*$ evolution for proportional strain (a) and biaxial (b) tests. The start and end points are marked by triangles and squares, respectively. A linear fit is shown for the dilatant proportional strain tests and repeated on the biaxial tests, as all the proportional strain tests converge towards a master curve.

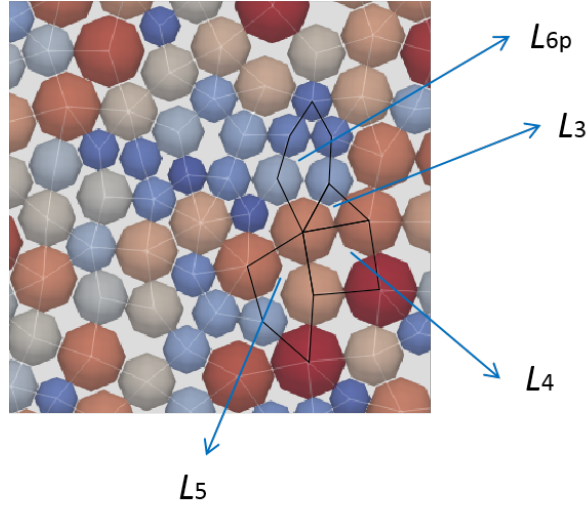
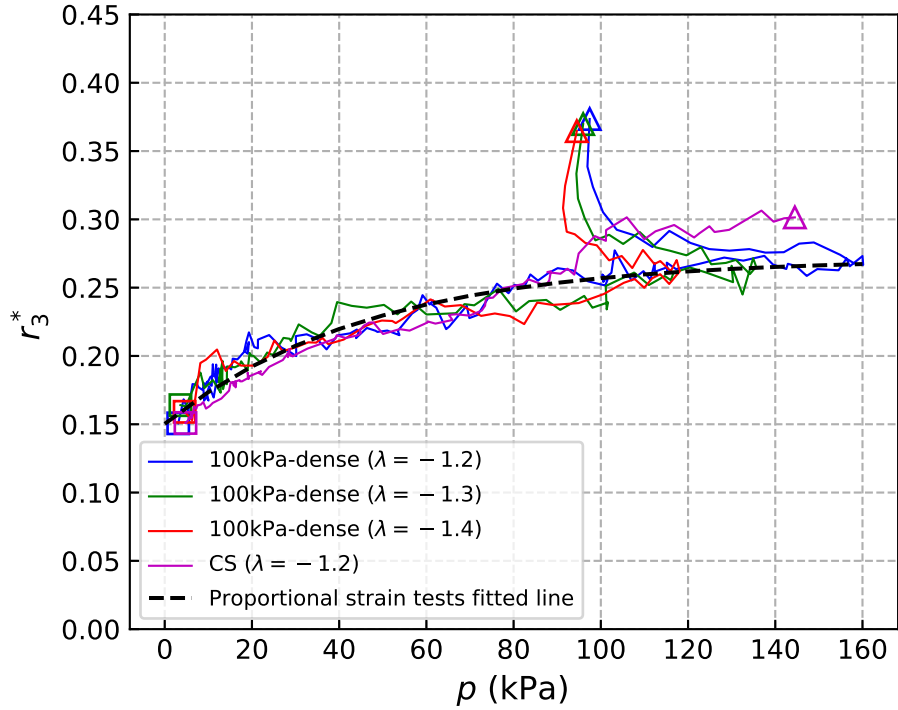


Figure 11: Meso-loop definition in granular materials

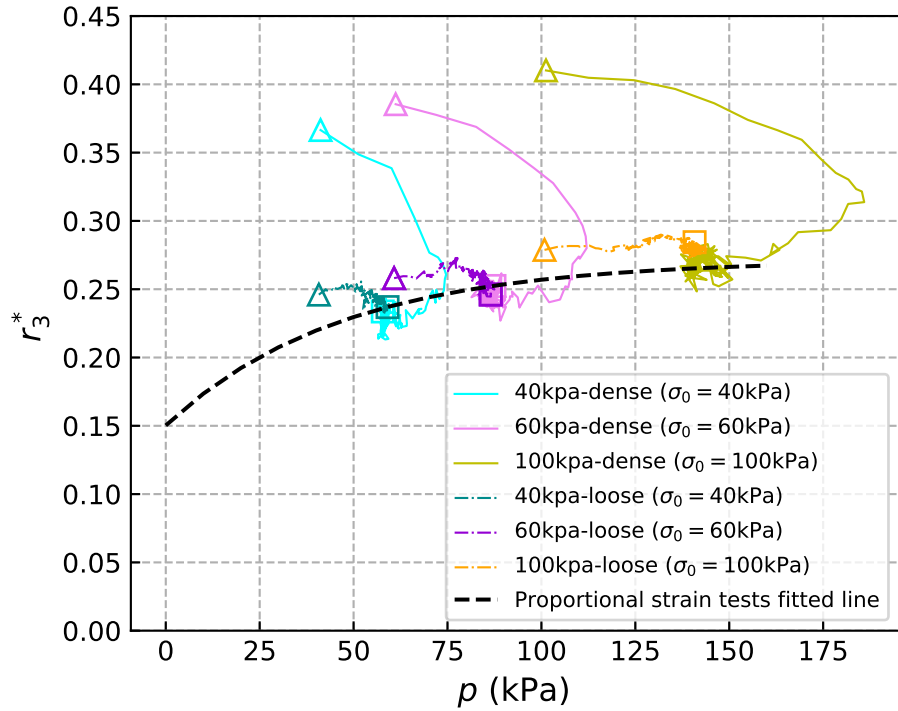
390 contacts investigated are exactly the same.

391

392 The evolution of α_c^* has been plotted in Fig.10 with respect to mean stress p . Except
 393 for the proportional strain loading starting from the CS, all the specimens have similar
 394 fabric characteristics in terms of variable α_c^* close to 0 at the initial states, due to the
 395 isotropic initial states where the inter-particle contact normal direction distribution is
 396 uniform in all the possible directions. As shown in Fig.10 (a), all $\alpha_c^* - p$ graphs from
 397 the proportional strain tests converge towards a master curve. A linear fit is given for
 398 the proportional strain tests and repeated in Fig.10 (b) to compare with the results
 399 from the biaxial tests. The relation between proportional strain tests and biaxial tests
 400 characterized by (p, q, e^*) has also been observed in the $p - \alpha^*$ plane, namely, the master
 401 curve obtained in proportional strain tests has gathered the critical states from biaxial
 402 tests. More importantly, all specimens under biaxial and proportional strain loading
 403 paths end up with the same anisotropy in the ultimate regime. The convergent feature
 404 at ultimate states along different loading paths is in line with the findings reported in the
 405 literature [12, 13].

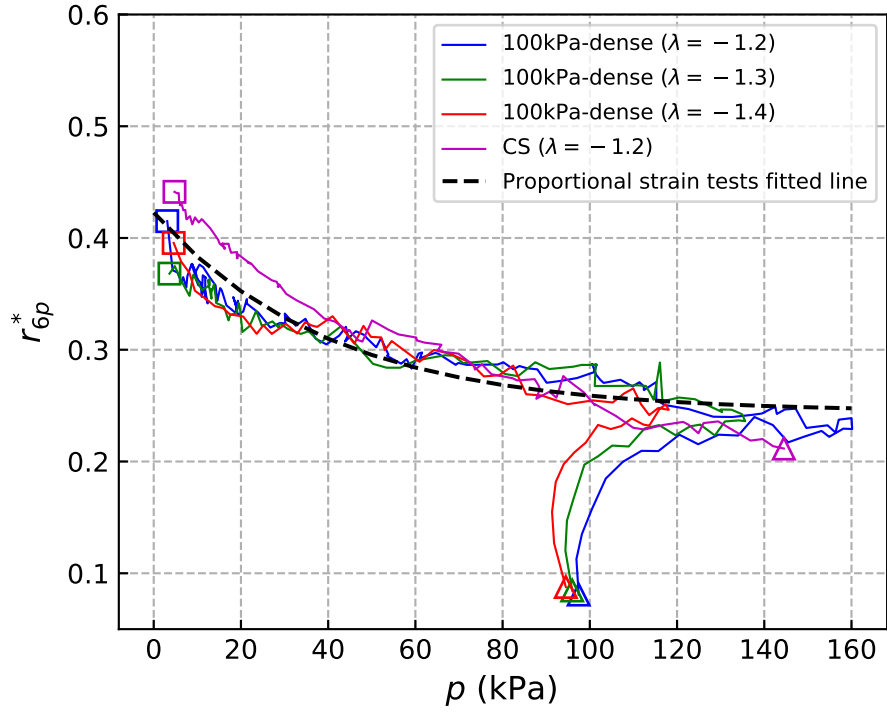


(a)

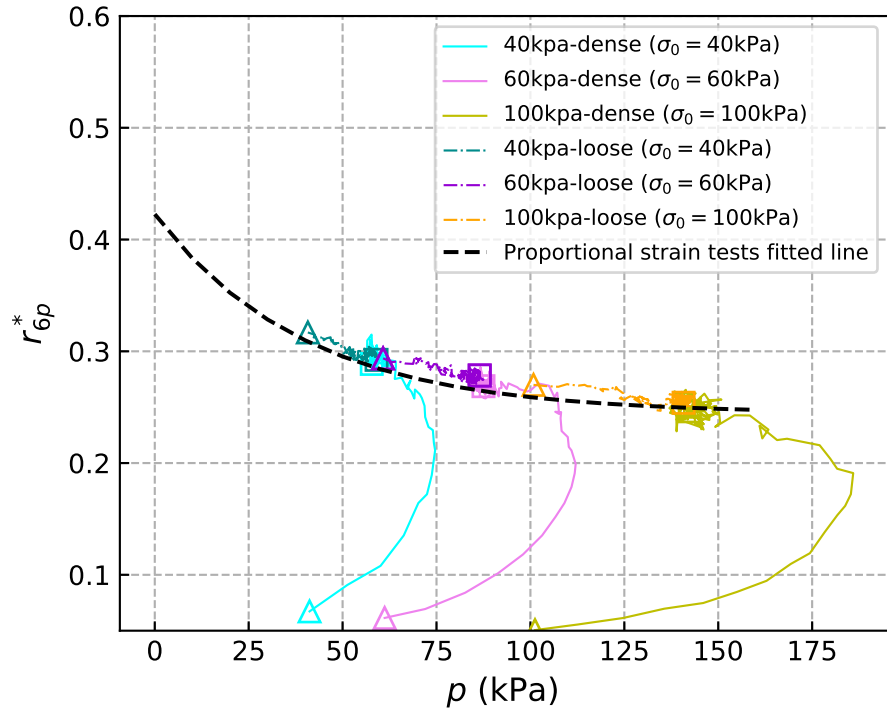


(b)

Figure 12: $p - r_3^*$ for proportional strain (a) and biaxial (b) test. The start and end points are marked by triangles and squares, respectively. An exponential fit is shown for the dilatant proportional strain tests and repeated on the biaxial tests, as all the proportional strain tests converge towards a master curve.

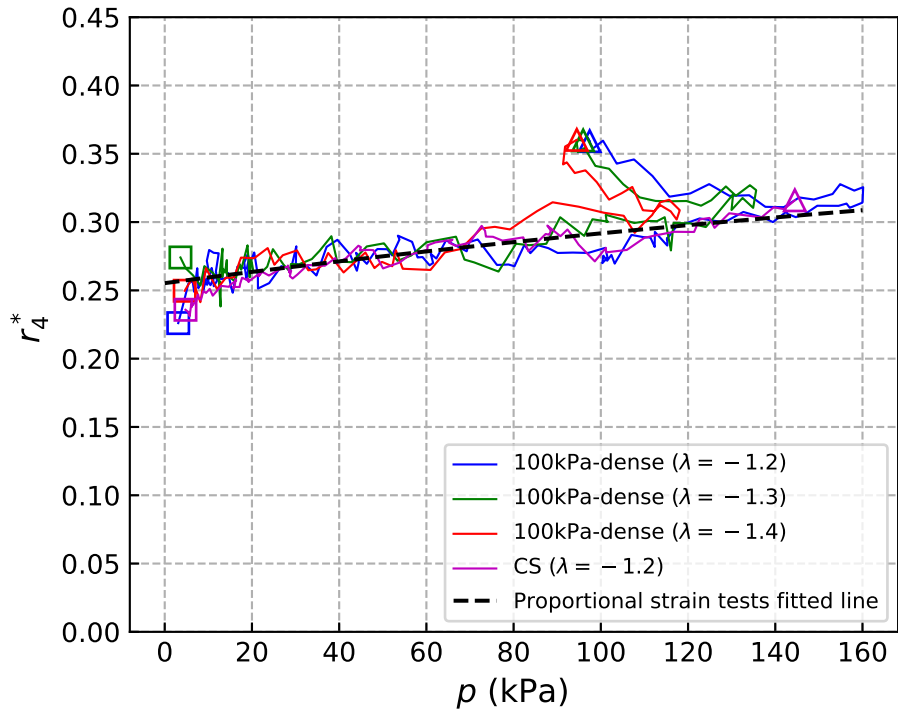


(a)

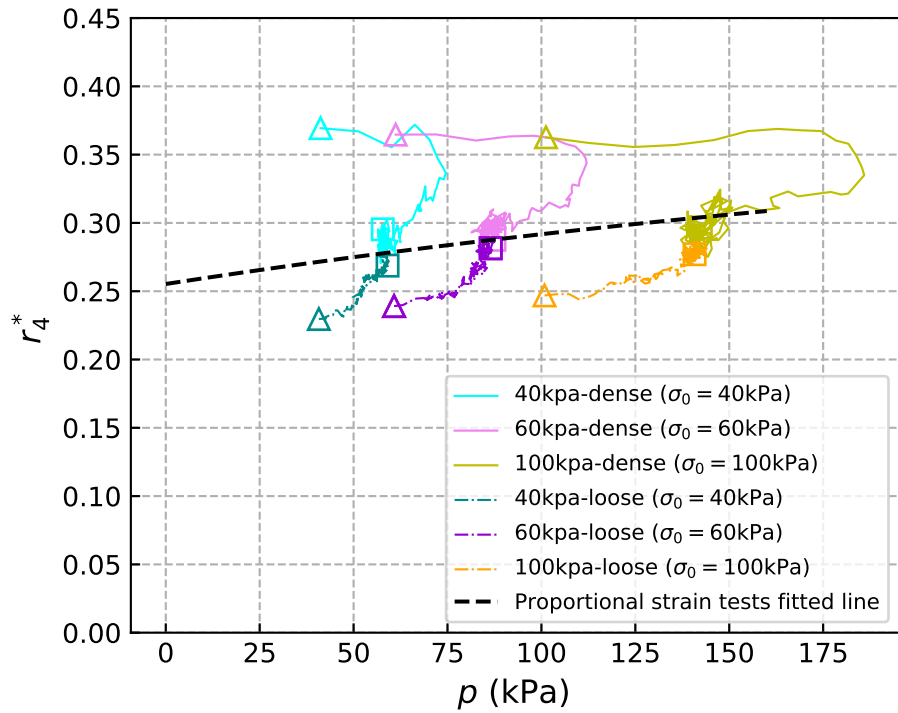


(b)

Figure 13: $p - r_{6p}^*$ for proportional strain (a) and biaxial (b) tests. The start and end points are marked by triangles and squares, respectively. An exponential fit is shown for the dilatant proportional strain tests and repeated on the biaxial tests, as all the proportional strain tests converge towards a master curve.

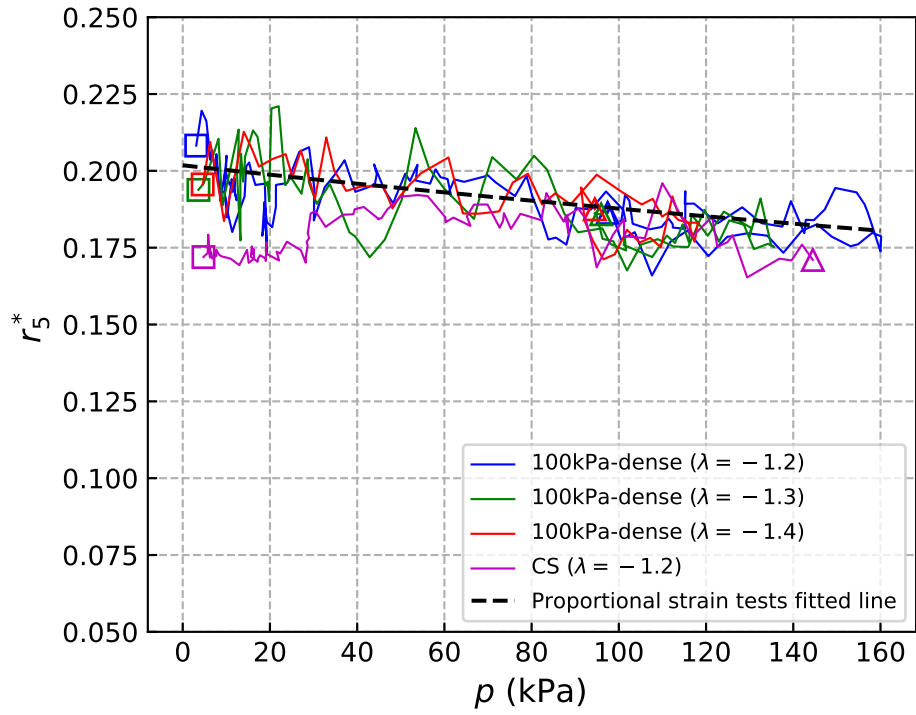


(a)

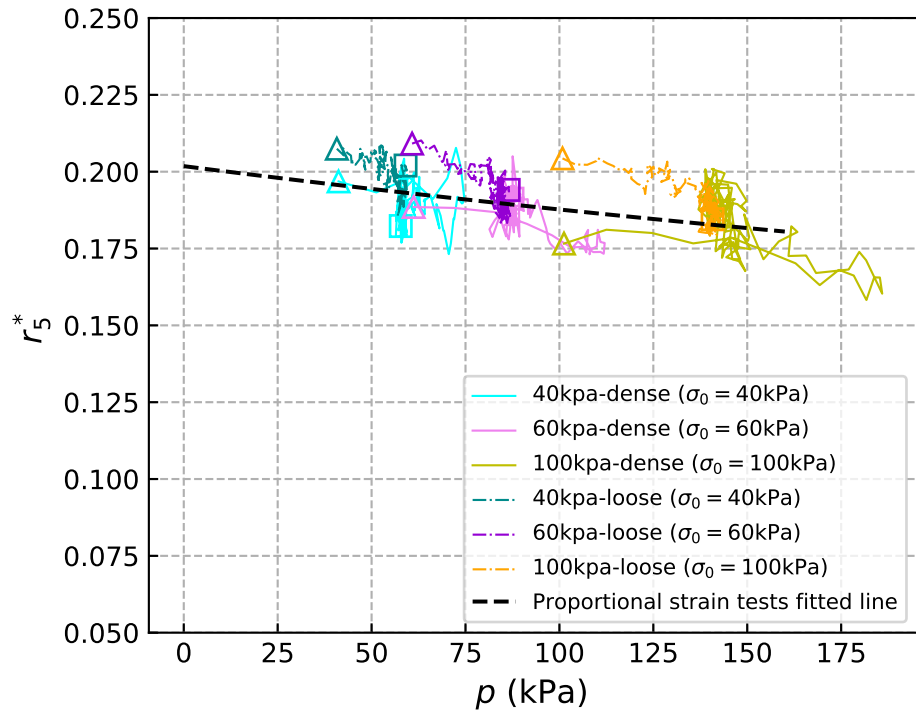


(b)

Figure 14: $p - r_4^*$ for proportional strain (a) and biaxial (b) test. The start and end points are marked by triangles and squares, respectively. An exponential fit is shown for the dilatant proportional strain tests and repeated on the biaxial tests, as the all proportional strain tests converge towards a master curve.



(a)



(b)

Figure 15: $p - r_5^*$ for proportional strain (a) and biaxial (b) test. The start and end points are marked by triangles and squares, respectively. An exponential fit is shown for the dilatant proportional strain tests and repeated on the biaxial tests, as all the proportional strain tests converge towards a master curve.

5.2 Meso-loop evolution

To obtain richer information on the critical state, we have analysed meso-loop related indexes in this subsection. As illustrated in Fig.11, meso-loops, enclosed by contact branches, are formed by tessellating the material area [36]. The side number of the loop influences considerably its deformability. In this section, loops will be categorized into four groups according to the side number, referred to as l_i ($i \in [3, 4, 5, 6p]$), where '6p' refers to a side number equal to or greater than 6. The percentages of categories are given by $r_i = n_i/n_t$, where n_i is the population of the meso-loop with a side number equal to i , and n_t refers to the total population of loops. It is worth noting that the reason for categorizing r_{6p} is that r_{7p} (percentage of categories with a side number equal or greater than 7) evolves in a similar way as r_6 [48]. The evolution of r_i^* ($i \in [3, 4, 5, 6p]$) within the shear band for dense specimens and the whole area for loose specimens is tracked along both the dilatant proportional strain loading path and the biaxial loading path.

The results as function of the mean stress p are presented in Fig.12 - 15. Small triangles and squares highlight the start and the end points of the curves and a fitting curve is given based on proportional strain tests in each figure. Two significant characteristics manifest themselves again: (1) the measures of r_i^* ($i \in [3, 4, 5, 6p]$) from proportional strain tests converge to form a master curve independent of the value of λ ; (2) the master curve agrees very well with the critical states characterized by the meso-loop indexes obtained in biaxial tests. These results are in agreement with the premise of ACST.

For the shortest loop l_3 , r_3^* continuously decreases from the initial to the ultimate point along all different loading paths. As for the most deformable type of loop l_{6p} , it is in a quite different situation as shown in Fig.13. The value of r_{6p}^* for the dense samples

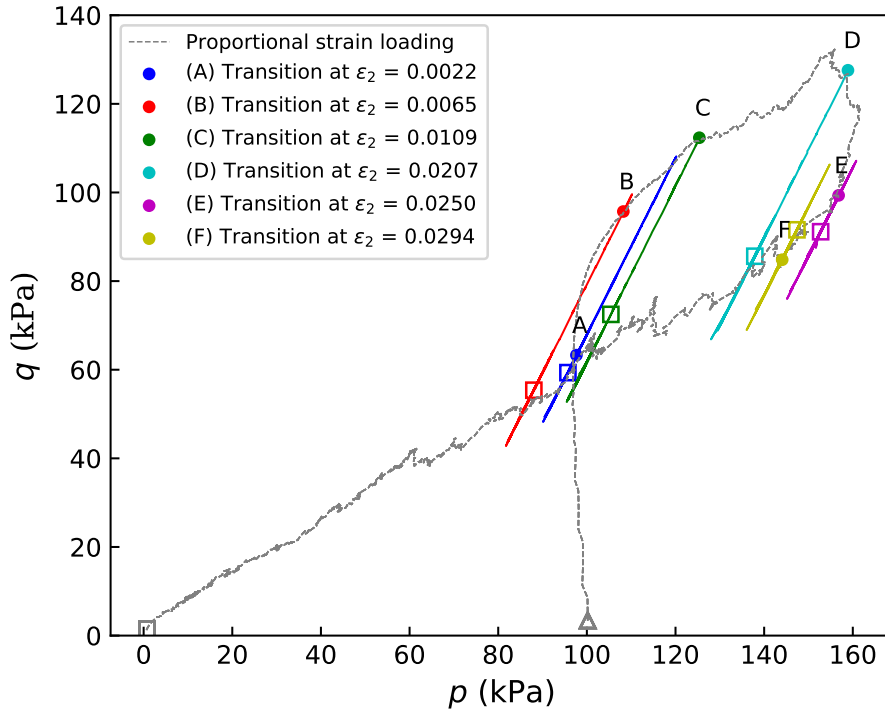


Figure 16: $p - q$ evolution along combining proportional strain and biaxial loading paths. The proportional strain loading with $\lambda = -1.2$ are conducted at first until a certain axial strain level labeled as A, B, C, D, E and F, after that a biaxial loading is performed by keeping the corresponding lateral stress unchanged. The transition states and the average critical states are marked by dots and squares, respectively. The corresponding stress-strain responses are shown in Fig.17

431 increases during loading, but it decreases for the loose samples.

432

433 Different to the fabric tensor based on the statistics of inter-particle contact normals,
 434 investigated in Subsection 5.1, that has been widely accepted as a quantitative measure
 435 of fabric anisotropy in granular materials [21], the scalar r_i^* is rather a measure charac-
 436 terizing the deformability of granular materials, namely the void ratio. Unlike the fabric
 437 anisotropy normalized by the specific volume [21], the evolution of r_i^* depends on p as
 438 illustrated in Fig.12 - 15.

439

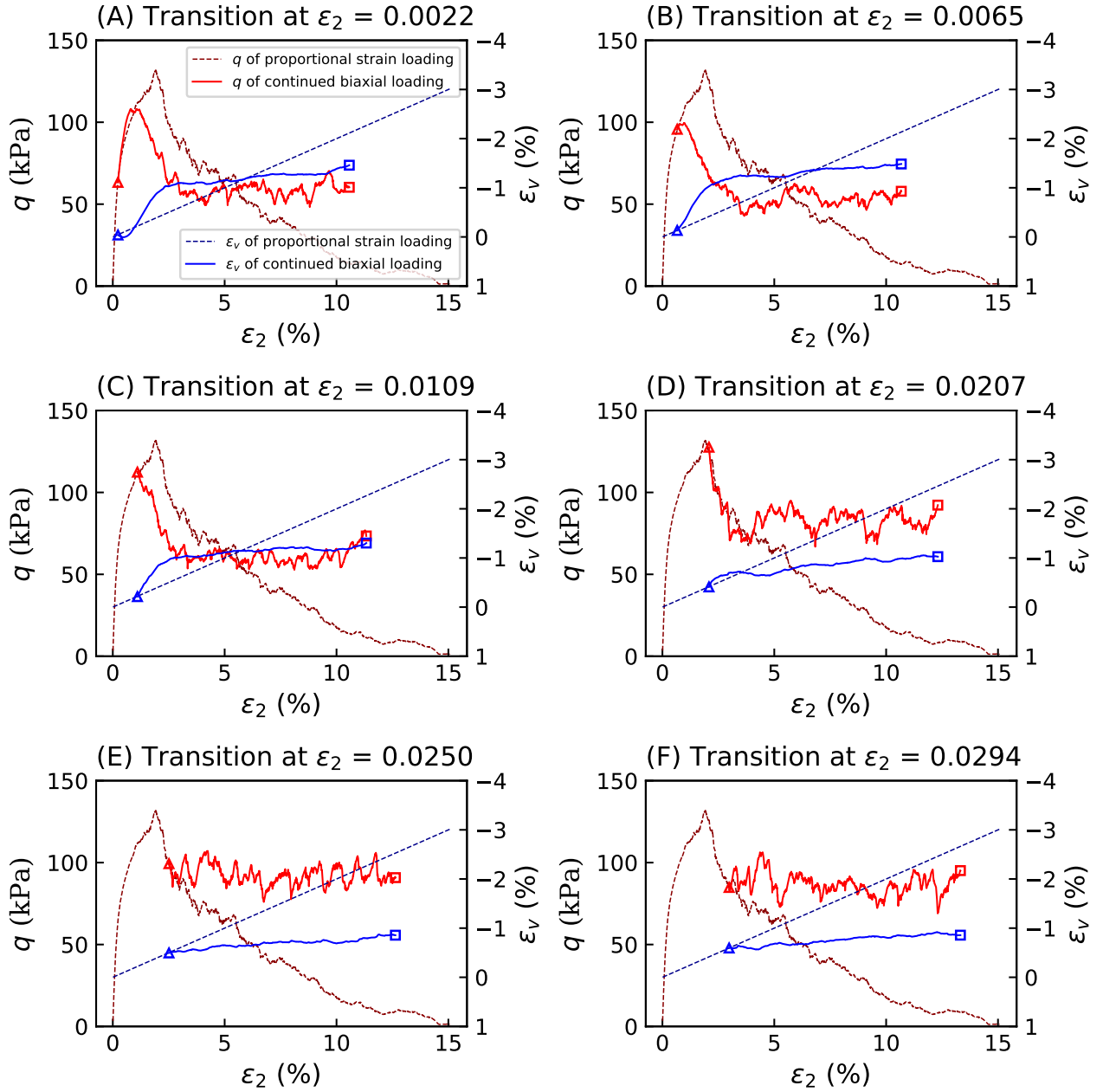


Figure 17: Stress-strain responses along combining proportional strain and biaxial loading paths. The switch states and ultimate states are marked by dots and squares, respectively. The corresponding stress paths are shown in Fig.16

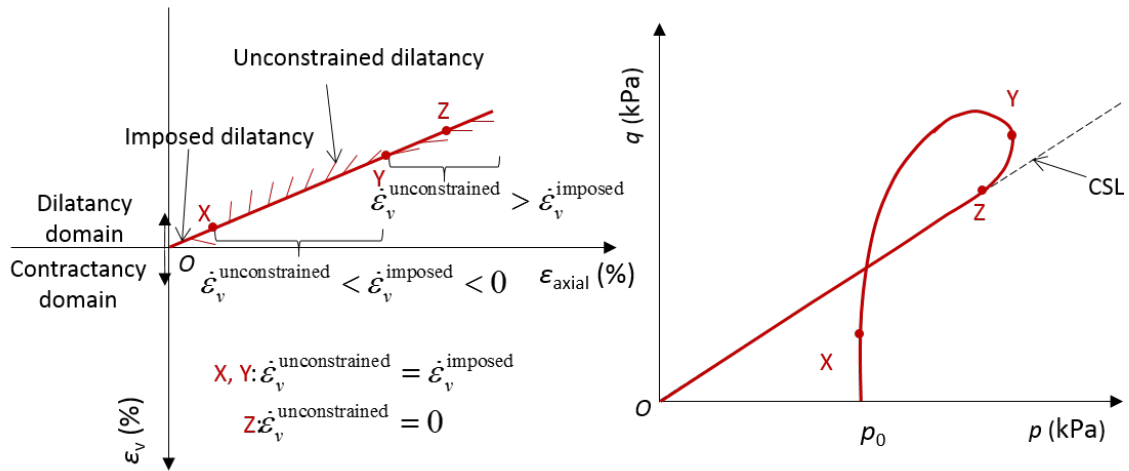


Figure 18: The relation between imposed dilatancy from proportional strain test and unconstrained dilatancy if switched to a biaxial condition according to results in Fig.16 and Fig.17. Note that soil mechanics convention is adopted with positive compression.

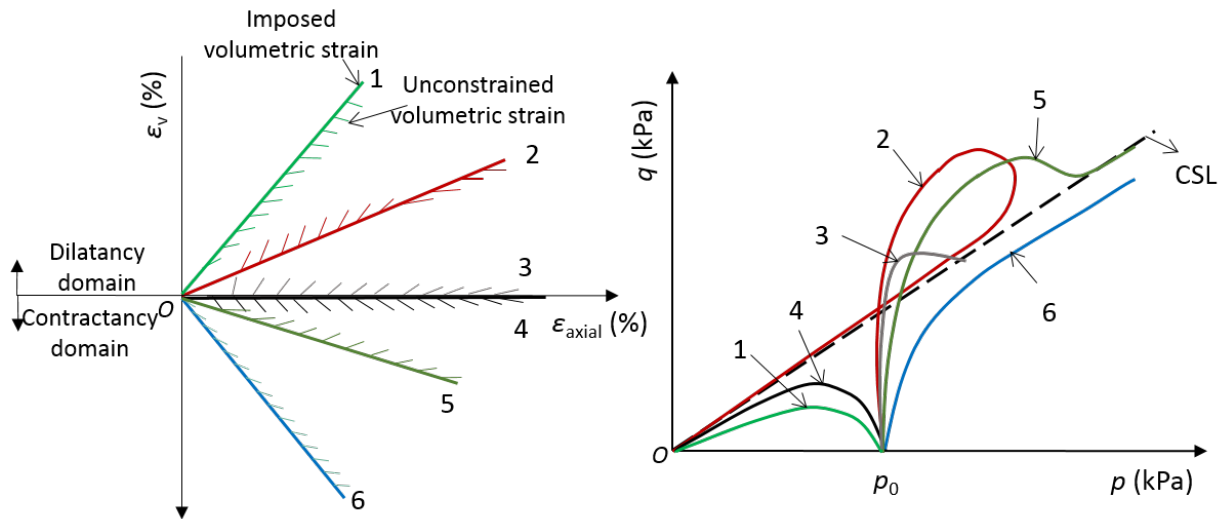


Figure 19: The relation between imposed dilatancy/contractancy in proportional strain tests and unconstrained dilatancy/contractancy expected in biaxial tests in the plane of axial strain vs. volumetric strain (left) and the possible stress paths in the plane of deviatoric stress vs. mean stress (right). The major solid lines represent the imposed dilatancy/contractancy, namely the proportional strain loading paths; the fins denote the incremental unconstrained dilatancy/contractancy if the loading is switched to biaxial conditions.

6 Mixed proportional strain and biaxial loading paths

A complex loading path combining proportional strain and biaxial paths has been simulated to confirm that proportional strain tests can indeed determine the position of critical state in the $e - p - q$ space as shown in Fig.6 and Fig.9. It was conducted as follows: first, the proportional strain path with $\lambda = -1.2$ was imposed; six groups of state data at $\varepsilon_2 = 0.0022, 0.0065, 0.0109, 0.0250$ and 0.0294 were selected; then, a biaxial loading path was performed at each state while the lateral stress was maintained as it was. Such mixed loading paths allow us to assess the existence of critical states according to the definition given in the introduction (continuous shearing with no change in volume or mean pressure, while keeping aligned stress anisotropy with fabric anisotropy). The stress paths along the mixed paths are shown in Fig.16, while the stress and strain responses are presented in Fig.17.

In Fig.16, the six transition states are labelled A, B, C, D, E and F and are marked by zoomed dots. The average critical (p, q) state is marked by squares. It can be observed that all six squares from continued biaxial tests lie along the stress track of proportional strain tests. As seen in Fig.17, when the loading path was adjusted to a biaxial test at $\varepsilon_2 = 0.0022$, a small compaction, followed by a large dilatancy, appears before a steady regime was reached; when the biaxial test was imposed at $\varepsilon_2 = 0.0065$ or 0.0109 , the volume increased at first before it reached a steady state; when $\varepsilon_2 = 0.0250$ or 0.0294 , the following biaxial loading path fluctuated around constant values for both deviatoric stress and volumetric strain, which means that the switching points correspond to a critical state. The stress-strain evolution of biaxial tests further proves that at relatively large

464 deformation, the proportional strain loading path will evolve along the critical state line
465 defined in biaxial tests.

466

467 Based on the results in Figures 16 and 17, the definition of critical state can be ex-
468 pressed as follows: *for a sample with fixed stress and strain rate directions, a $p - q - e$*
469 *state is considered as a critical state if the application of a biaxial loading under the same*
470 *lateral pressure, starting from this $p - q - e$ state, leads to zero volume strain and zero*
471 *deviatoric stress evolution.* Note that for such a state, a rotation of the principal stress
472 direction with p and q constant will nevertheless result in a change of e . This result
473 observed for instance in [41] shows that the critical state cannot be described only by the
474 three internal state variables $p - q - e$; additional variables related to the micro-structural
475 anisotropy due to loading direction are necessary to define a state equation for the critical
476 state line [22].

477

478 Figures 16 and 17 also provide information for comparing the *unconstrained dilatancy*
479 obtained in biaxial tests with the *imposed dilatancy* in proportional strain tests ⁱⁱ. As
480 illustrated in Fig.18, the solid line represents the imposed dilatancy with respect to axial
481 strain. The fixed dilatant rate is characterized by the slope of the line. The fins give the
482 unconstrained dilatancy rate (namely a direction of incremental volumetric strain), that
483 would be observed if the loading were switched to a biaxial one. At the beginning, the
484 imposed dilatancy is larger than the unconstrained dilatancy (from point O to X), the
485 mean stress p decreases slightly from p_0 to X . When the imposed dilatancy is smaller than
486 the unconstrained dilatancy expressed as $\dot{\epsilon}_v^{\text{unconstrained}} < \dot{\epsilon}_v^{\text{imposed}} < 0$ (from point X to Y),
487 the stress response p increases from X to Y . The unconstrained dilatancy decreases contin-

ⁱⁱNote that the terms *unconstrained* and *imposed* are used to recall that the volumetric strain is a response variable in a biaxial loading while it is a control variable in proportional strain tests.

488 uously thanks to the imposed dilatancy. The states at $\varepsilon_2 = 0.0065$ and 0.0109 in Fig.17
 489 belong to this domain. At points X and Y, where the unconstrained dilatancy equals
 490 the imposed dilatancy, the mean stress p reaches the peak. The state at $\varepsilon_2 = 0.0207$ in
 491 the proportional strain test is close to point Y. After point Y, the unconstrained dila-
 492 tancy decreases continuously to become smaller than the imposed dilatancy, described as
 493 $0 > \dot{\varepsilon}_v^{\text{unconstrained}} > \dot{\varepsilon}_v^{\text{imposed}}$ till zero unconstrained dilatancy at point Z ($\dot{\varepsilon}_v^{\text{unconstrained}} = 0$).
 494 At point Z, the stress path reaches the CSL defined by biaxial tests. If a biaxial path is
 495 followed after point Z, $\dot{\varepsilon}_v^{\text{unconstrained}} = 0$ occurs as shown in the results from mixed tests
 496 switched at $\varepsilon_2 = 0.0250$ and 0.0294 . The further imposed dilatancy after point Y leads
 497 the stress path to turn back to approach point O along the CSL. In conclusion, when the
 498 imposed dilatancy is smaller (larger) than the unconstrained dilatancy, the mean stress p
 499 increases (decreases).

500

501 The results in Fig.7 suggest that the relation between imposed dilatancy/contractancy
 502 in proportional strain tests and dilatancy/contractancy expected in biaxial tests can be
 503 categorized as shown in Fig.19. The strain path 1 represents a situation for which the im-
 504 posed dilatancy is larger than the unconstrained dilatancy (contractancy can be regarded
 505 as the negative dilatancy) from the beginning. This strain path leads to a liquefaction
 506 presented as stress path 1. Dilatant proportional strain loading path 2 leads to a more
 507 complex response, as discussed before.

508

509 The proportional strain test with zero volume change (often referred to as undrained
 510 test) can be categorized as one of two types, depending on whether $\dot{\varepsilon}_v^{\text{unconstrained}} < 0$ at
 511 the beginning (path 3) or $\dot{\varepsilon}_v^{\text{unconstrained}} > 0$ (path 4). The unconstrained dilatancy along
 512 loading path 3 tends toward zero (horizontal direction), when approaching the critical

513 state. Conversely, loading path 4, representing an isochoric test on a loose sample, results
514 in liquefaction.

515

516 As for the contracting proportional strain path, two groups can be identified according
517 to whether the stress path crosses the CSL as paths 5 and 6 do. At the beginning of curve
518 5, the unconstrained contractancy being larger than the imposed contractancy, the mean
519 stress p decreases slightly. Shortly afterwards, the unconstrained contractancy becomes
520 smaller than the imposed contractancy, which leads to the increase in p . The direction of
521 the fins tending to become horizontal is synchronized with the $p - q$ curve approaching
522 the CSL when strain localization takes place within the sample. The representation of
523 curve 5 is based on results from simulations of mixed biaxial/contracting proportional
524 strain loading paths (these results are not presented in this paper whose focus is upon
525 dilatant proportional strain loading paths). Curve 6 represents the situation where the
526 unconstrained contractancy is always smaller than the imposed contractancy, which leads
527 to a continuous increase in p .

528

529 To summarize, the mean stress will increase in the dilatancy domain, when the im-
530 posed dilatancy rate is smaller than the unconstrained dilatancy rate. When the imposed
531 dilatancy is larger than the unconstrained dilatancy, the mean stress decreases and tends
532 to 0 for large volumetric strain. When the imposed dilatancy is first smaller and then
533 larger than the unconstrained dilatancy, the stress path is likely to undergo a stress loop.
534 In the contractancy domain, when the imposed contractancy is larger than the uncon-
535 strained contractancy, the mean stress increases. On the other hand, an imposed con-
536 tractancy being smaller than the unconstrained contractancy will result in a decrease in p .

537

538 These numerical findings can also be interpreted in terms of dilatancy angles if we
 539 recall that the dilatancy angle is defined in 2D by $\sin\psi = \dot{\epsilon}_v/\dot{\epsilon}_d = \dot{\epsilon}_v/(2\dot{\epsilon}_{\text{axial}} - \dot{\epsilon}_v)$.
 540 As long as it can be assumed that granular materials follow a standard non-associated
 541 elasto-plastic behavior (which is true in 2D or axisymmetric conditions for instance[28]),
 542 the dilatancy angle characterize the flow rule, and the unconstrained dilatancy can be
 543 viewed as a material property. This broadens the scope of the analysis summarized in
 544 Figure 19 insofar, as making it independent of the loading paths considered (at least for
 545 2D or axisymmetric conditions). The present results are also consistent with previous
 546 experimental and theoretical studies [8, 9]. In [8], the dilatancy rate defined by $\dot{\epsilon}_v/\dot{\epsilon}_{\text{axial}}$
 547 can be related to the effective mean pressure. In the criterion of liquefaction given in [9],
 548 the dilatancy angle obtained from the flow rule and the mean pressure at a given initial
 549 void ratio have a non-linear negative correlation.

550

551 7 Conclusion and outlook

552 By simulating proportional strain tests, biaxial tests and complex loading paths combin-
 553 ing biaxial and proportional strain paths using DEM, we have explored through a series of
 554 mechanical and fabric indexes the relation between proportional strain tests and critical
 555 states from biaxial tests.

556

557 In considering the results obtained from biaxial tests, we have observed that all struc-
 558 tural variables (e^* , α_c^* , r_i^*) within shear bands for specimens experiencing a localized kine-
 559 matic pattern will converge to the same values as for specimens experiencing a diffuse
 560 kinematic pattern at critical state along the same biaxial loading path. These results

561 are consistent with the conclusion drawn by Zhu et al. [48] that localization and diffuse
562 patterns share the same fabric properties.

563

564 As for proportional strain tests, when the dilatant rate is relatively small and the
565 axial strain is large enough, a stress path in the $p - q$ plane will finally reach the critical
566 state line defined by biaxial tests after experiencing a stress loop. The curves on the $p - e^*$
567 (void ratio), $p - \alpha_c^*$ (fabric anisotropy intensity defined from contact normal direction) and
568 $p - r_i^*$ (population of meso-loops) planes also converge towards a master curve regardless
569 of the magnitude of dilatancy characterized by $\lambda = -1.2, -1.3, -1.4$. In combining these
570 results, it can be inferred that any dilatant volume change will always result in similar
571 $(p, q, e^*, \alpha_c^*, r_i^*)$ states after the material memory has been erased.

572

573 More interestingly is the relation observed between the mechanical states reached
574 along a proportional strain test and the critical states obtained from biaxial tests within
575 the framework of ACST. Macroscopic responses (p, q, e^*) and fabric-related measures
576 (α_c^*, r_i^*) in homogeneous domains along biaxial tests evolve towards the evolution curve
577 of those variables from proportional strain tests at critical state. Given these results,
578 only one single test is therefore necessary to construct the classical critical state line in
579 $(p - q - e^* - \alpha_c^* - r_i^*)$ space for any granular material. Therefore, the CS concept can be
580 generalized to a wide class of loading paths which shows that CS acts as a general at-
581 tractor irrespective of the loading path considered. This idea of proportional strain paths
582 enriched considerably the data base for confirmation of CST and ACST.

583

584 The mixed proportional strain and biaxial loading paths also confirm this relation. A
585 more general definition of CS can be given as follows: a $p - q - e$ state, for a sample with

586 constant stress and strain rate directions, after a given loading history, is considered at
587 critical state if the application of a biaxial loading under the same lateral pressure start-
588 ing from this $p-q-e$ state leads to zero volume strain and zero deviatoric stress evolution.

589

590 In addition, the comparison between the imposed dilatancy/contractancy along pro-
591 portional strain paths and unconstrained dilatancy/contractancy expected along biaxial
592 paths provides valuable information to the interpretation of the various loading paths
593 obtained in $p-q$ plane for proportional strain loading paths. Along proportional strain
594 tests, the volumetric strain, which tends to be steady, produces the stress path approach-
595 ing the CSL.

596

597 Proportional strain loading paths are attracted by the critical state line. For sam-
598 ples initially at critical state (after a biaxial loading for instance), a proportional strain
599 loading imposes the evolution of the sample state along the critical state line. Even for
600 samples not initially at critical state, when subjected to proportional strain loading, the
601 micro-structure rearranges itself and reaches geometrical arrangements corresponding to
602 critical state. This memory fading is probably a key ingredient affecting complex systems
603 and may also be at the origin of emerging properties. It will be of great interest to further
604 investigate the underpinning mechanisms of memory fading according to the kinematic
605 pattern (localization vs. diffuse mode). In addition, from a microscopic point of view,
606 critical state is a dynamic equilibrium, where only statistics are constant. Most consti-
607 tutive models for granular materials describe the critical state from a phenomenological
608 point of view ignoring the micro-mechanical dynamics. Allowing critical state to emerge
609 in micro-mechanical constitutive models from a physical viewpoint will provide a chal-
610 lenging topic for the future. One limitation of this study is that all conclusions above are

611 drawn based on 2D simulations. The extension to 3D, numerically and experimentally,
612 will be attempted in the future.

613

614 **Acknowledgement**

615 The authors wish to thank Professor Félix Darve (3SR) for insightful discussions and
616 his valuable comments and suggestions on how to improve this work. The authors also
617 thank Dr. Jiaying Liu (Wuhan University) for her valuable comments. The authors
618 express their sincere thanks to the French Research Network GeoMech (GDRI CNRS)
619 for promoting positive and convivial interactions among researchers. The support from
620 China Scholarship Council (CSC) under the Grant CSC Number 201801810030 and from
621 the BRGM (French geological Survey) under the contract RP19DRP023 is gratefully
622 acknowledged. The constructive comments by the reviewers are highly appreciated.

623 **References**

- 624 [1] K. Been and M. G. Jefferies. A state parameter for sands. *Géotechnique*, 35(2):99–
625 112, 1985.
- 626 [2] K. Been, M. G. Jefferies, and J. Hachey. Critical state of sands. *Géotechnique*,
627 41(3):365–381, 1991.
- 628 [3] A. Casagrande. Characteristics of cohesionless soils affecting the stability of slopes
629 and earth fills. *Journal of the Boston Society of Civil Engineers*, 23(1):13–32, 1936.

- 630 [4] J. Chu, S. C. Lo, and I. K. Lee. Strain-softening behavior of granular soil in strain-
631 path testing. *Journal of Geotechnical Engineering*, 118(2):191–208, 1992.
- 632 [5] P. A. Cundall and O. D. Strack. A discrete numerical model for granular assemblies.
633 *Géotechnique*, 29(1):47–65, 1979.
- 634 [6] F. Da Cruz, S. Emam, M. Prochnow, J.-N. Roux, and F. Chevoir. Rheophysics of
635 dense granular materials: Discrete simulation of plane shear flows. *Physical Review*
636 *E*, 72(2):021309, 2005.
- 637 [7] A. Daouadji, P.-Y. Hicher, M. Jrad, B. Sukumaran, and S. Belouettar. Experimen-
638 tal and numerical investigation of diffuse instability in granular materials using a
639 microstructural model under various loading paths. *Géotechnique*, 63(5):368–381,
640 2013.
- 641 [8] A. Daouadji, M. Jrad, G. Robin, A. Brara, and E. M. Daya. Phase transforma-
642 tion states of loose and dense granular materials under proportional strain loading.
643 *Journal of Engineering Mechanics*, 143(1):C4016007, 2017.
- 644 [9] F. Darve. Liquefaction phenomenon of granular materials and constitutive stability.
645 *Engineering Computations: Int J for Computer-Aided Engineering*, 13(7):5–28, 1996.
- 646 [10] J. Desrues, R. Chambon, M. Mokni, and F. Mazerolle. Void ratio evolution in-
647 side shear bands in triaxial sand specimens studied by computed tomography.
648 *Géotechnique*, 46(3):529–546, 1996.
- 649 [11] A. Drescher and G. D. J. De Jong. Photoelastic verification of a mechanical model
650 for the flow of a granular material. *Journal of the Mechanics and Physics of Solids*,
651 20(5):337–340, 1972.

- 652 [12] P. Fu and Y. F. Dafalias. Fabric evolution within shear bands of granular materials
653 and its relation to critical state theory. *International Journal for Numerical and*
654 *Analytical Methods in Geomechanics*, 35(18):1918–1948, 2011.
- 655 [13] P. Fu and Y. F. Dafalias. Relationship between void- and contact normal- based
656 fabric tensors for 2d idealized granular materials. *International Journal of Solids*
657 *and Structures*, 63:68–81, 2015.
- 658 [14] Z. Gao, J. Zhao, X. S. Li, and Y. F. Dafalias. A critical state sand plasticity model
659 accounting for fabric evolution. *International Journal for Numerical and Analytical*
660 *Methods in Geomechanics*, 38(4):370–390, 2014.
- 661 [15] E. Ibraim, J. Lanier, D. Muir Wood, and G. Viggiani. Strain path controlled shear
662 tests on an analogue granular material. *Géotechnique*, 60(7):545–559, 2010.
- 663 [16] R. Kawamoto, E. Andò, G. Viggiani, and J. E. Andrade. All you need is shape:
664 Predicting shear banding in sand with ls-dem. *Journal of the Mechanics and Physics*
665 *of Solids*, 111:375–392, 2018.
- 666 [17] N. P. Kruyt and L. Rothenburg. On micromechanical characteristics of the criti-
667 cal state of two-dimensional granular materials. *Acta Mechanica*, 225(8):2301–2318,
668 2014.
- 669 [18] N. P. Kruyt and L. Rothenburg. A micromechanical study of dilatancy of granular
670 materials. *Journal of the Mechanics and Physics of Solids*, 95:411–427, 2016.
- 671 [19] X. Li and X. S. Li. Micro-macro quantification of the internal structure of granular
672 materials. *Journal of Engineering Mechanics*, 135(7):641–656, 2009.

- 673 [20] X. S. Li. Modeling of dilative shear failure. *Journal of Geotechnical and Geoenvi-*
674 *ronmental Engineering*, 123(7):609–616, 1997.
- 675 [21] X. S. Li and Y. Dafalias. Dissipation consistent fabric tensor definition from DEM
676 to continuum for granular media. *Journal of the Mechanics and Physics of Solids*,
677 78:141–153, 2015.
- 678 [22] X. S. Li and Y. F. Dafalias. Anisotropic critical state theory: role of fabric. *Journal*
679 *of Engineering Mechanics*, 138(3):263–275, 2012.
- 680 [23] X. S. Li, Y. F. Dafalias, and Z. L. Wang. State dependant dilatancy in critical-state
681 constitutive modelling of sand. *Canadian Geotechnical Journal*, 36(4):599–611, 1999.
- 682 [24] J. Liu, F. Nicot, and W. Zhou. Sustainability of internal structures during shear
683 band forming in 2d granular materials. *Powder Technology*, 338:458–470, 2018.
- 684 [25] J. Liu, A. Wautier, S. Bonelli, F. Nicot, and F. Darve. Macroscopic softening in
685 granular materials from a mesoscale perspective. *International Journal of Solids and*
686 *Structures*, 2020.
- 687 [26] J. Liu, W. Zhou, G. Ma, S. Yang, and X. Chang. Strong contacts, connectivity and
688 fabric anisotropy in granular materials: A 3d perspective. *Powder Technology*, 2020.
- 689 [27] F. Nicot, A. Daouadji, N. Hadda, M. Jrad, and F. Darve. Granular media failure
690 along triaxial proportional strain paths. *European Journal of Environmental and*
691 *Civil Engineering*, 17(9):777–790, 2013.
- 692 [28] F. Nicot and F. Darve. Basic features of plastic strains: from micro-mechanics to
693 incrementally nonlinear models. *International Journal of Plasticity*, 23(9):1555–1588,
694 2007.

- 695 [29] F. Nicot and F. Darve. Diffuse and localized failure modes: two competing mecha-
696 nisms. *International Journal for Numerical and Analytical Methods in Geomechanics*,
697 35(5):586–601, 2011.
- 698 [30] F. Nicot and F. Darve. The H microdirectional model: accounting for a mesoscopic
699 scale. *Mechanics of Materials*, 43(12):918–929, 2011.
- 700 [31] F. Nicot, N. Hadda, M. Guessasma, J. Fortin, and O. Millet. On the definition of
701 the stress tensor in granular media. *International Journal of Solids and Structures*,
702 50(14-15):2508–2517, 2013.
- 703 [32] F. Nicot, L. Sibille, and P.-Y. Hicher. Micro–macro analysis of granular material be-
704 havior along proportional strain paths. *Continuum Mechanics and Thermodynamics*,
705 27(1-2):173–193, 2015.
- 706 [33] C. O’Sullivan, J. D. Bray, and S. Li. A new approach for calculating strain for
707 particulate media. *International Journal for Numerical and Analytical Methods in*
708 *Geomechanics*, 27(10):859–877, 2003.
- 709 [34] K. Roscoe, A. Schofield, and C. Wroth. On the yielding of soils. *Géotechnique*,
710 8(1):22–53, 1958.
- 711 [35] E. Salvatore, G. Modoni, E. Andò, M. Albano, and G. Viggiani. Determination of
712 the critical state of granular materials with triaxial tests. *Soils and Foundations*,
713 57(5):733–744, 2017.
- 714 [36] M. Satake. A discrete-mechanical approach to granular materials. *International*
715 *journal of engineering science*, 30(10):1525–1533, 1992.

- 716 [37] A. Schofield and P. Wroth. *Critical State Soil Mechanics*, volume 310. McGraw-Hill
717 London, 1968.
- 718 [38] J. Shi and P. Guo. Induced fabric anisotropy of granular materials in biaxial tests
719 along imposed strain paths. *Soils and Foundations*, 58(2):249–263, 2018.
- 720 [39] L. Sibille, N. Hadda, F. Nicot, A. Tordesillas, and F. Darve. Granular plasticity,
721 a contribution from discrete mechanics. *Journal of the Mechanics and Physics of*
722 *Solids*, 75:119–139, 2015.
- 723 [40] V. Smilauer, E. Catalano, B. Chareyre, S. Dorofeenko, J. Duriez, N. Dyck, J. Elias,
724 B. Er, A. Eulitz, A. Gladky, et al. Yade documentation 2nd ed., 2015.
- 725 [41] A. I. Theocharis, E. Vairaktaris, Y. F. Dafalias, and A. G. Papadimitriou. Necessary
726 and sufficient conditions for reaching and maintaining critical state. *International*
727 *Journal for Numerical and Analytical Methods in Geomechanics*, 43(12):2041–2055,
728 2019.
- 729 [42] R. Verdugo and K. Ishihara. The steady state of sandy soils. *Soils and Foundations*,
730 36(2):81–91, 1996.
- 731 [43] R. Wan, F. Nicot, and F. Darve. *Failure in Geomaterials: a Contemporary Treatise*.
732 Elsevier, 2017.
- 733 [44] R. G. Wan and P. J. Guo. Stress dilatancy and fabric dependencies on sand behavior.
734 *Journal of Engineering Mechanics*, 130(6):635–645, 2004.
- 735 [45] A. Wautier, S. Bonelli, and F. Nicot. Dem investigations of internal erosion: Grain
736 transport in the light of micromechanics. *International Journal for Numerical and*
737 *Analytical Methods in Geomechanics*, 43(1):339–352, 2019.

- 738 [46] Z.-Y. Yin and C. S. Chang. Stress–dilatancy behavior for sand under loading and
739 unloading conditions. *International Journal for Numerical and Analytical Methods
740 in Geomechanics*, 37(8):855–870, 2013.
- 741 [47] J. Zhao and N. Guo. Unique critical state characteristics in granular media consid-
742 ering fabric anisotropy. *Géotechnique*, 63(8):695, 2013.
- 743 [48] H. Zhu, H. N. Nguyen, F. Nicot, and F. Darve. On a common critical state in
744 localized and diffuse failure modes. *Journal of the Mechanics and Physics of Solids*,
745 95:112–131, 2016.